Liner fleet deployment and speed optimization under emission reduction technologies

Dan Zhuge
School of Management, Shanghai University, Shanghai 200444, China, dan_zhuge@shu.edu.cn

Jingwen Wu
School of Management, Shanghai University, Shanghai 200444, China, jingwen_wu@shu.edu.cn

Lu Zhen*
School of Management, Shanghai University, Shanghai 200444, China, lzhen@shu.edu.cn

Shuaian Wang
Faculty of Business, The Hong Kong Polytechnic University, Hung Hom 999077, Hong Kong, wangshuaian@gmail.com

Yu Wang
School of Management, Shanghai University, Shanghai 200444, China, wangyu202206@163.com

Maritime shipping faces stringent exhaust emission requirements due to sulfur emission regulations and the European Union Emissions Trading System (EU ETS), driving shipping companies to adopt a range of emission reduction technologies, such as scrubbers, liquefied natural gas (LNG) propulsion systems, and methanol propulsion systems. Given that many shipping companies operate fleets equipped with multiple emission reduction technologies, this study investigates an integrated fleet deployment and speed optimization problem for a shipping company operating three or more types of ships (traditional ships, scrubber-equipped ships, and LNG- or methanol-powered ships) under sulfur emission regulations and the EU ETS carbon emission regulation. A mixed-integer nonlinear programming (MINLP) model is proposed to address this optimization problem. Due to their differing regulatory mechanisms, sulfur and carbon emission regulations affect fleet deployment (i.e., the types and number of ships deployed across all routes) and speed optimization in distinct ways. As the number of ship types increases, the number of feasible fleet deployment plans grows sharply, while the inclusion of different ship types further complicates speed optimization, increasing the overall problem complexity. To tackle this challenge, the study performs mathematical derivations and analyses to reveal model properties and construct valid inequalities, significantly narrowing the feasible solution space. The MINLP model is first linearized according to its characteristics. Leveraging the model properties, a Benders decomposition algorithm with a tailored cut pool is developed to solve the linearized model, which serves as the foundation for a highly efficient exact algorithm for the original MINLP model. Numerical experiments show that the proposed exact algorithm achieves a nearly 90-fold reduction in computation time compared with the CPLEX-based algorithm.

Key words: Fleet deployment; speed optimization; sulfur emission regulations; European Union Emissions Trading System; emission reduction technologies

* Corresponding author

1. Introduction

The maritime shipping industry supports approximately 90% of all international trade (Park et al. 2022). According to UNCTAD (2023), international marine trade is predicted to continue growing at a rate of 2.1%–2.2% from 2024 to 2028. However, the growth of maritime trade is also a significant contributor to environmental pollution. Shipping activities generate substantial exhaust gases, such as sulfur oxides (SO_x) and carbon dioxide (CO_2)(Zhuge et al. 2024). To address the pressing issue of ship emissions, the International Maritime Organization (IMO) and the European Union (EU) have implemented stringent emission control measures. The IMO has identified several specific regions as Emission Control Areas (ECAs) to curb sulfur emissions, with the Baltic Sea, North Sea, North American, United States Caribbean Sea, and Mediterranean Sea ECAs already in effect, while the Canadian Arctic, Norwegian Sea, and North-East Atlantic Ocean ECAs have been approved and are scheduled to take effect in 2027 and 2028. Ships operating within these ECAs must adhere to a stringent sulfur content limit of 0.1% in their fuel, whereas those navigating outside these areas are permitted to use fuel with a sulfur content of up to 0.5%. According to the EU Directive, since January 1, 2024, the shipping industry has been included in the European Union Emissions Trading System (EU ETS). This measure requires shipping companies operating on EU routes and intra-EU routes to purchase and surrender carbon allowances for CO_2 emissions from cargo and passenger ships of 5,000 GT and above. Specifically, for voyages departing from EU ports to non-EU ports (e.g., Rotterdam to Shanghai) and voyages departing from non-EU ports to EU ports (e.g., Shanghai to Rotterdam), a payment is required for 50% of the carbon emissions of the voyage. For voyages between EU ports (e.g., Hamburg to Marseille), the full amount of emissions must be accounted for.

In response to increasingly stringent environmental regulations, the vast majority of mid-to-large-sized shipping companies operate mixed fleets comprising traditional ships, scrubber-equipped ships, and alternative-fuel-powered ships (Wang et al. 2025a). Compliance with sulfur- and carbon-related regulations has raised operating costs through both higher fuel expenses (e.g., switching to cleaner fuels such as MGO in regulated areas) and capital/operational expenditures associated with emission-control technologies (e.g., scrubbers). Relative to the previous sulfur emission standards, the current regulations imply a significant increase in fuel-related costs for traditional ships. Illustratively, the fuel cost premium associated with sulfur compliance can reach approximately 300 US$/ton within ECAs and around 100 US$/ton outside ECAs, reflecting the price differentials between compliant and non-compliant fuels (Ship and Bunker 2024). In addition, the introduction of carbon emission regulations under the EU ETS further increases the operating costs of shipping companies. Under these current emission regulations, how to deploy different ship technologies across service routes and how to

operate them (e.g., speed choices inside vs. outside ECAs) has become a critical practical planning problem rather than a purely theoretical question. Shipping companies need to strategically implement these emission reduction technologies while maintaining cost-effective operations. Fuel switching is widely adopted for traditional ships due to its operational simplicity. Scrubbers remove sulfur from exhaust gases, allowing ships to meet sulfur limits while continuing to use lower-cost high-sulfur fuel oil (HSFO) within ECAs. Alternatively, switching to LNG or methanol can satisfy sulfur regulations and potentially reduce carbon emissions, but typically requires substantial retrofit investment (Chen et al. 2018b). These technology choices also interact with operational decisions. For traditional ships, operators often reduce speed inside ECAs to limit expensive MGO consumption, but then increase speed outside ECAs to maintain fixed liner schedules, which can increase fuel burn and CO_2 emissions. By contrast, scrubber-equipped ships burning HSFO tend to operate at a more stable speed profile across legs, while alternative-fuel-powered ships trade lower emissions for higher fixed or capital-related costs. These trade-offs—ship fixed costs, fuel consumption, emission control, and speed management—are tightly coupled across routes and ship types. Given that mixed fleets are already commonplace, developing a quantitative framework that jointly optimizes fleet deployment and speed strategies is both necessary and practically relevant, providing decision support for operational planning under realistic regulatory constraints.

Motivated by the above-mentioned real-world challenge in green shipping, this study contributes to liner operations management by introducing a mixed-integer nonlinear programming (MINLP) model for integrated fleet deployment and speed optimization under multiple emission reduction technologies. This model provides shipping companies with a scientific approach to decision-making on how to deploy different types of ships and how to adjust speed on each leg of each route under sulfur and carbon emission regulations. Sulfur and carbon emission regulations impose different types of restrictions, leading to distinct impacts on fleet deployment (i.e., the types and number of ships deployed across all routes) and speed optimization. Meanwhile, the presence of multiple ship types results in a vast number of deployment plans, significantly increasing the computational complexity of the problem. When different ship types are assigned to the same route, although their optimal sailing speeds differ, their speeds must be mutually adjusted to maintain a common service schedule. Hence, fleet deployment on each route is further affected by both the ship types and the coordinated sailing speeds. These factors collectively pose significant computational difficulties for solving the model efficiently. To address this, we first analyze the problem structure to derive key model properties and valid inequalities that help reduce the solution space of feasible fleet deployment plans. The MINLP model is then linearized according to its characteristics, and selected model properties

are embedded into both the master and subproblems within a Benders decomposition framework. This enables the development of a tailored Benders decomposition algorithm that efficiently solves the linearized model for large-scale instances, forming the basis of a highly efficient exact algorithm for the original MINLP model.

The practical relevance of the proposed optimization model and exact algorithm is demonstrated through analytical properties derived from the model and computational experiments based on approximated real-world data, which together yield a range of managerial insights relevant for shipping companies operating under increasingly stringent environmental regulations. In particular, the identified characteristics of optimal sailing speeds within and outside ECAs on each leg provide guidance for speed design in practice. The derived upper bound on the optimal number of ships deployed on each route offers a useful reference for shipping companies by improving the efficiency of fleet deployment decision making. Moreover, the sensitivity analysis with respect to fuel prices illustrates how the optimal ship type and number decisions may change under different market conditions, thereby supporting fleet deployment planning under realistic operational scenarios. When calibrated with company-specific data, the proposed model and algorithm constitute an implementable decision-support framework with interpretable outputs, including fleet deployment and leg-level speed decisions. Owing to its high computational efficiency, the framework can support cost-effective operational planning even for large-scale liner shipping networks under environmental regulations.

The contributions of this study are threefold. First, addressing a practical challenge faced by many shipping companies, this study is the first to simultaneously optimize fleet deployment and sailing speed under both sulfur and carbon emission regulations involving three or more ship types, through the formulation of an MINLP model. Second, sulfur and carbon emission regulations have distinct effects on fleet deployment and speed decisions; feasible deployment plans increase sharply with the number of ship types, and incorporating multiple ship types further complicates speed optimization, increasing overall problem complexity. To overcome these difficulties, this study derives key mathematical properties and develops valid inequalities for the proposed model, effectively eliminating a large number of non-optimal fleet deployment plans and obtaining the optimal sailing speed characteristics. Finally, this study linearizes the MINLP model and proposes a tailored Benders decomposition algorithm that exploits its key properties. A highly efficient exact algorithm based on the tailored Benders decomposition algorithm is then designed for the original MINLP model. Numerical experiments demonstrate that the proposed exact algorithm reduces computation time by nearly 90 times compared with the CPLEX solver.

The remainder of this paper is organized as follows. Section 2 provides a comprehensive literature review. Section 3 presents an MINLP model for the fleet deployment and speed optimization

problem under emission reduction regulations and technologies. Section 4 describes the solution method, including the derivation of valid inequalities and the design of an exact algorithm for the MINLP model, based on its properties and Benders decomposition. Computational experiments are conducted in Section 5 to derive managerial insights. The conclusions are then outlined in the final section.

2. Literature review

This study focuses on the integrated optimization of fleet deployment and ship speed under multiple emission reduction technologies. The relevant literature can be categorized into three research streams: fleet deployment, speed optimization, and emission reduction technologies.

The fleet deployment problem is a fundamental planning task in liner shipping, which involves assigning available vessels to predetermined routes to minimize operational costs. Comprehensive reviews are provided by Meng et al. (2014), Lee and Song (2017), and Christiansen et al. (2020). Early research mainly addressed basic fleet deployment problems, focusing on issues such as incomplete demand information (Ng and Lin 2018), stochastic container weights (Zhen et al. 2019), and network adjustments under varying market conditions (Wetzel and Tierney 2020). In recent years, a growing number of papers focus on heterogeneous fleet deployment. For example, Wang and Wang (2021) consider optimizing deployment, sequencing, and scheduling for heterogeneous ships on a shipping route, achieving a 5% cost reduction compared to homogeneous fleets. Wang et al. (2025c) explore co-management of heterogeneous fleet in alliances and formulate an MINLP model to maximize profits while ensuring fairness in resource sharing. Wu et al. (2023) further address multi-period heterogeneous fleet deployment under uncertainty, incorporating repositioning and adaptive fleet sizes. They formulate a mixed-integer linear programming model and propose a Benders-based branch-and-cut algorithm for this problem. In contrast to the above study that uses stochastic programming to capture uncertainty, Xiang et al. (2024) and Wang et al. (2025b) further explore robust optimization for the heterogeneous fleet deployment problem under uncertainty and propose the column-and-constraint generation (CCG) algorithm. Zhao et al. (2024) emphasize schedule reliability by combining heterogeneous ship deployment with conditional value-at-risk (CVaR) to mitigate delay risks. Environmental regulations, such as the ECAs, Energy Efficiency Existing Ship Index (EEXI), and Carbon Intensity Indicator (CII), have reshaped fleet deployment strategies in liner shipping. Wang et al. (2021) highlight the operational and cost challenges posed by ECA regulations, which mandate the use of low-sulfur fuel, necessitating integrated optimization of fleet deployment and schedule design. Zhang et al. (2024b) demonstrate that CII regulations lead to reduced ship speeds and carbon emissions, albeit with potential increases in fleet size, while EEXI has a limited impact due to widespread slow steaming.

The sailing speed optimization problem focuses on finding the optimal cruising speeds for ships by balancing factors such as the number of ships needed for services, fuel consumption, and the quality of service offered to customers (Wang and Wang 2016). Based on ship voyage report data, Du et al. (2019) propose a two-phase framework for speed and trim optimization using neural networks. Ge et al. (2021) introduce a net present value framework to investigate the properties of optimal speeds. Considering the oil consumption of ships is treated as a cubic function of speeds, Wang and Zhao (2022) develop a probabilistic tabu search algorithm for container liner speed optimization. Optimizing sailing speed is an economical approach to enhance ship energy efficiency and a practical solution for meeting emission reduction targets (Luo et al. 2024). Zhuge et al. (2021) address the complex issue of optimizing ship path, speed, and deployment in liner shipping, considering the impact of sulfur emission regulations, carbon taxes, and ship speed reduction incentive programs on operational costs. Considering the impact of CII regulations on speed optimization in tramp shipping, Cheng et al. (2025) integrate cargo selection, route planning, and speed adjustment to minimize emissions and costs while complying with CII standards. Luo et al. (2024) propose an innovative ship sailing speed optimization method that incorporates dynamic meteorological conditions to reduce fuel consumption, highlighting its potential to support the IMO's emissions reduction targets by optimizing speeds in the absence of real-time weather data. Some studies also analyze the effect of ECAs on speed optimization. For example, Lee et al. (2023) propose a stochastic dynamic programming model to optimize the speed, trim and path decisions of ships inside and outside ECAs considering uncertain weather conditions. Zhen et al. (2024) develop a mathematical programming model from the regulator's viewpoint to optimize ECA width and sulfur limits, while incorporating a shipping liner's response model to determine optimal speeds. While existing studies often examine the effects of sulfur or carbon emission regulations separately, the different fuels required within and outside ECAs already influence the speed decisions of traditional ships, and the introduction of carbon emission costs under the EU ETS further incentivizes speed reductions across the entire voyage to control overall costs. Therefore, under both sulfur and carbon emission regulations, sailing speeds must be optimized in an integrated manner to balance emission reductions and operational cost efficiency.

Several emission reduction technologies, such as fuel switching, scrubber installation, and LNG-powered ships, are available under sulfur emission regulations and the EU ETS. Zis et al. (2022) analyze the economic and environmental implications of green technology adoption, particularly focusing on scrubbers. Their results suggest that scrubbers are more profitable under higher fuel prices and longer sailing times. Zhang et al. (2024a) investigate the selection of green fuels and technologies for a coastal container ship and establish the necessary and sufficient conditions for

adopting a scrubber installation strategy, which depends on factors such as equivalent sailing distance, fuel price ratios, and scrubber specifications. Zeng et al. (2024) further examine the impact of different speed adjustment behaviors on the efficiency of scrubbers. This study categorizes speed adjustment into rigid, partial, and full flexibility. Many studies consider the optimization of multiple emission reduction technologies, compared to the above studies that consider only one emission reduction technology. For example, Zhen et al. (2020) conduct a study of green technology adoption (i.e., scrubbers and shore power) for fleet deployment in a shipping network. Ma et al. (2023) propose an energy strategy selection model based on life cycle analysis to investigate multiple green technology adoption. Considering the relatively low adoption rate of green technologies in inland waterway transport, Shao et al. (2024) study the adoption of green fuels and green technologies for a given fleet of inland river carriers. Further influenced by the EU ETS regulation, Zhou et al. (2025) develop economic models and simulations to investigate how the allocation of emission allowances influences shipowners' choices of emission reduction technologies. Despite the progress made, most existing studies still consider only one or two ship types equipped with emission reduction technologies. As the diversity of ship types increases, the trade-offs among operational costs, fuel choices, and emission compliance become markedly more complex. These limitations underscore the need for a more general modeling framework that can accommodate multiple ship types and incorporate emission-related decisions directly into the fleet deployment process.

Table 1 Comparison between this study and closely related studies

Literature	Emission regulation		Emission reduction technology				Operational decision		Solution method
	Sulfur (ECA)	Carbon (EU ETS)	Fuel switching	Scrubber	LNG	Other technologies	Fleet deployment	Sailing speed	
Zhen et al. (2020)	✓			✓			✓	✓	TPH
Wang et al. (2021)	✓		✓				✓	✓	TA; DP
Zhuge et al. (2021)	✓		✓				✓	✓	DP
Lee et al. (2023)	✓		✓	✓				✓	DA
Ma et al. (2023)	✓		✓	✓	✓			✓	DP
Zeng et al. (2024)	✓		✓	✓				✓	Analytical
Zhang et al. (2024a)	✓		✓	✓				✓	Analytical
This study	✓	✓	✓	✓	✓	✓	✓	✓	BDMP

Notes: TPH: Three-phase heuristic; TA: Tailored algorithm; DP: Dynamic programming; DA: Desrochers' algorithm; BDMP: Benders decomposition with model properties.

Table 1 presents a comparison between this study and closely related literature on fleet deployment and speed optimization under multiple emission reduction technologies. The literature has yet to systematically explore how to simultaneously address fleet deployment,

speed optimization, and the adoption of different green technologies within sulfur and carbon regulatory frameworks. In particular, existing research rarely considers heterogeneous fleets comprising three or more ship types, each equipped with distinct emission reduction technologies. Moreover, research that comprehensively analyzes how sulfur and carbon emission regulations jointly influence fleet operations remains scarce. These gaps limit our ability to capture the operational and fleet-related complexities that shipping companies face under increasingly stringent regulatory requirements. From a methodological perspective, incorporating these factors substantially increases decision-making complexity, and no prior study has developed an exact algorithm capable of effectively addressing this challenge.

This study develops a novel MINLP model to fill these gaps, integrating fleet deployment and speed optimization under multiple emission reduction technologies while incorporating realistic sulfur and carbon emission regulations. These integrated decisions pose significant modeling and computational challenges. The inclusion of carbon emission coefficients under the EU ETS introduces non-trivial interactions with sulfur emission regulations, creating a tightly coupled problem. Coordinating fleet deployment and speed decisions across heterogeneous ships and multiple routes further increases complexity, resulting in an MINLP model whose size grows sharply with the number of ship types. To address these challenges, the study derives key model properties and develops valid inequalities, which are embedded within a tailored Benders decomposition framework to efficiently solve the piecewise-linearized model. Building on this tailored Benders decomposition algorithm, we further design an exact algorithm for the original MINLP model. The proposed model and algorithm are suitable for large-scale shipping networks and can assist shipping companies in balancing cost efficiency and regulatory compliance.

3. Model formulation

We investigate an integrated fleet deployment and speed optimization problem for a liner shipping company with $|R|$ service routes and $|I|$ ($|I| \geq 3$) types of ships under sulfur and carbon emission regulations. Route $r \in R$ represents a round trip, consisting of a series of calling ports (collected in set L_r), arranged in a given sequence. A leg $l \in L_r$ is defined as a sailing from port of call l to port of call $(l+1)$. The sailing distances within and outside ECAs on leg $l \in L_r$ of route $r \in R$ are represented by d_{rl}^E and d_{rl}^N, respectively. Each service route maintains a weekly service frequency, guaranteeing that each port of call is visited once on the same day every week. The round-trip duration of a route therefore depends on its ship deployment plan. The ship deployment plan on route $r \in R$ involves the number of different types of ships deployed on the route, i.e., the number of type-i ($i \in I$) ships deployed on route $r \in R$, denoted as q_{ir}. The number of ships for each type $i \in I$ is denoted as Q_i. We define the total port time at all ports of call on route $r \in R$ as T_r. When

different types of ships are deployed on route $r \in R$, they must follow the same schedule, i.e., they have the same sailing time t_{rl} (in hours) on leg $l \in L_r$. We denote t^E_{irl} and t^N_{irl} as the sailing times for type-i ships within and outside ECAs on leg $l \in L_r$ of route $r \in R$, respectively.

Different types of ships are powered by different marine fuels: traditional ships use 0.1% sulfur fuel (e.g., marine gas oil [MGO]) within ECAs and 0.5% sulfur fuel (e.g., very low-sulfur fuel oil [VLSFO]) outside ECAs, scrubber-equipped ships use HSFO within and outside ECAs, and LNG-powered or methanol-powered ships use LNG or methanol on the whole voyage. The fuel prices of energy-equivalent fuel (to one ton of VLSFO) used within and outside ECAs for type-i ships on leg $l \in L_r$ of route $r \in R$ are represented by c^E_i and c^N_i, respectively, where $c^E_i \geq c^N_i$. The fuel consumption rate for type-i ships on leg $l \in L_r$ of route $r \in R$ is a convex function of speed, represented as $a \cdot v^b$, where a and b are conversion factors between fuel consumption per unit distance and speed, with $a > 0$ and $b > 1$, and v is the sailing speed. The fixed costs for different types of ships are also different, denoted as c^{fix}_i per type-i ship per week. Under the EU ETS, the cost of CO_2 emissions from burning energy-equivalent fuel (to one ton of VLSFO) for type-i ships on leg $l \in L_r$ of route $r \in R$ is represented by c^{car}_{irl}.

Sulfur emission regulations increase fuel costs for traditional ships within ECAs, prompting them to adjust their sailing speeds in response to the differing unit fuel prices within and outside ECAs to minimize total fuel cost. Scrubber-equipped ships use cheaper HSFO throughout but incur additional fixed costs for installing or retrofitting scrubbers. Alternative-fuel ships (e.g., LNG- or methanol-powered) also face substantial fixed costs due to newbuilding or retrofitting of alternative-fuel systems, and their fuel costs may be higher or lower than traditional fuels depending on the fuel type. These differences in fixed and fuel costs influence both fleet deployment and speed optimization. In addition, the incorporation of carbon emission costs under the EU ETS imposes a cost on the CO_2 emitted, which motivates ships to reduce sailing speeds both within and outside ECAs to mitigate overall cost increases (see Fig. 1(a)). The interactions between sulfur and carbon regulations create tightly coupled operational incentives. Since sailing speed is a key determinant of round-trip duration and thus the number of ships required to maintain weekly service frequency, there is a strong interdependence between fleet deployment and speed decisions. Therefore, sailing speed and fleet deployment must be optimized jointly to balance emission reduction and operational cost efficiency under both sulfur and carbon emission regulations.

Different ship types further complicate fleet deployment and sailing speed decisions. Strict sulfur emission regulations lead different ship types to adopt distinct speed profiles along a given leg. For example, traditional ships (type-1 ships) tend to vary their speeds within and outside ECAs, whereas scrubber-equipped ships maintain a relatively constant speed throughout the voyage. When a route is served by different types of ships, they must follow a unified schedule,

requiring coordinated speed adjustments. This coordination may force each type of ship to deviate from its optimal sailing speed, as in the example shown in Fig. 1(b). Speed adjustments influence schedule design, which in turn affects fleet deployment strategies. As a result, emission regulations may also alter the types of ships deployed, and the optimal number of ships can vary across deployment plans involving different ship types, as illustrated in Fig. 1(c). Moreover, when three or more ship types are considered, the fleet deployment and speed optimization problem becomes more complex due to greater heterogeneity in fuel consumption and emissions, necessitating a highly nonlinear and tightly coupled decision-making framework. The sharp increase in feasible deployment plans due to multiple ship types further complicates the optimization problem.

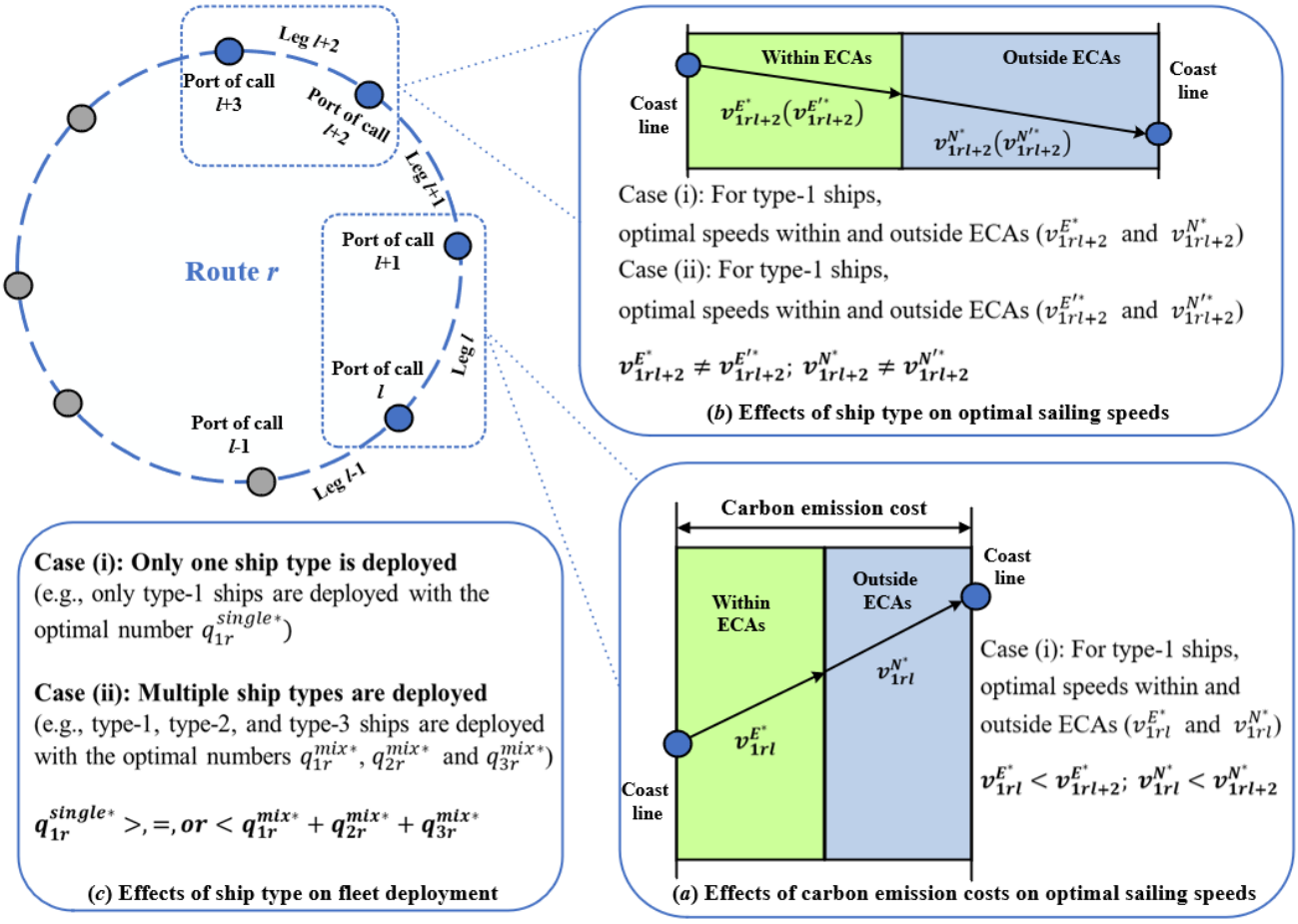

Figure 1 **Effects of multiple ship types and carbon emission cost**

To capture the vast number of fleet deployment plans and the complex interplay between fleet deployment and speed optimization across multiple ship types, while accounting for sulfur and

carbon emission regulations, this study develops an MINLP model aimed at minimizing total costs. Specifically, the total costs considered include the fixed costs of all ships, fuel costs across all routes, and carbon emission costs incurred under the EU ETS. Although scrubbers and cleaner energy sources can mitigate exhaust emissions, they come with higher fixed costs due to retrofitting expenses or increased newbuilding costs. Some alternative energy options also entail higher unit fuel costs compared to traditional fuels. Therefore, the primary challenge of this study lies in balancing fixed costs, fuel costs, and carbon emission costs. We summarize the main notation used in this study below.

Sets

I	Set of all ship types
P	Set of all ship type selection plans, each specifying the ship types deployed on all routes
R	Set of all routes
R_p^{single}	Set of all routes each with a single ship type under ship type selection plan $p \in P$
R_p^{mix}	Set of all routes each with more than one ship type under ship type selection plan $p \in P$
L_r	Set of all legs on route $r \in R$
$\mathbb{Z}_+$	Set of nonnegative integers

Parameters

a, b	Conversion factors between fuel consumption per unit distance and sailing speed for type-i ships: fuel consumption per unit distance for type-i ships is $a \cdot v^b$ (ton/nautical mile, i.e., ton/nm), where v is sailing speed (knots); $a > 0$ and $b > 1$
c_i^{fix}	Fixed cost (US$/week) of a type-$i$ ship
c_i^E	Price (US$) of energy-equivalent fuel (to one ton of VLSFO) used within ECAs for type-i ships
c_i^N	Price (US$) of energy-equivalent fuel (to one ton of VLSFO) used outside ECAs for type-i ships
c_{irl}^{car}	Cost (US$) of CO_2 emissions from burning energy-equivalent fuel (to one ton of VLSFO) within or outside ECAs for type-i ships on leg $l \in L_r$ of route $r \in R$
d_{rl}^E	Sailing distance (nm) within ECAs on leg $l \in L$ of route $r \in R$
d_{rl}^N	Sailing distance (nm) outside ECAs on leg $l \in L$ of route $r \in R$
Q_i	Total number of type-i ships
T	Hours in a week; $T = 168$ hours
T_r	Total time (hours) spent at all ports of call on route r
$V^{\max}$	Maximum speed (nm/hour) for ships

Decision variables

q_{ir}	Number of type-i ships deployed on route $r \in R$
t_{irl}^E	Sailing time (hours) within ECAs on leg $l \in L_r$ of route $r \in R$ for type-i ships
t_{irl}^N	Sailing time (hours) outside ECAs on leg $l \in L_r$ of route $r \in R$ for type-i ships

t_{rl} Sailing time (hours) on leg $l \in L_r$ of route $r \in R$

The integrated fleet deployment and speed optimization problem for the liner shipping company under sulfur and carbon emission regulations is formulated as

$$[\text{M1}]\ \min \sum_{i\in I}\sum_{r\in R} c_i^{\text{fix}} q_{ir} + \sum_{r\in R}\sum_{i\in I} \frac{q_{ir}}{\sum_{i'\in I} q_{i'r}} \sum_{l\in L_r} \left[(c_i^E + c_{irl}^{\text{car}}) d_{rl}^E \cdot a \left(\frac{d_{rl}^E}{t_{irl}^E} \right)^b + (c_i^N + c_{irl}^{\text{car}}) d_{rl}^N \cdot a \left(\frac{d_{rl}^N}{t_{irl}^N} \right)^b \right] \quad (1)$$

subject to

$$\sum_{i\in I} q_{ir} \cdot T = \sum_{l\in L_r} t_{rl} + T_r, \forall r \in R \quad (2)$$

$$t_{irl}^E + t_{irl}^N = t_{rl}, \forall i \in I, \forall r \in R, \forall l \in L_r \quad (3)$$

$$\sum_{r\in R} q_{ir} \le Q_i, \forall i \in I \quad (4)$$

$$t_{irl}^E \ge \frac{d_{rl}^E}{V^{\max}}, \forall i \in I, \forall r \in R, \forall l \in L_r \quad (5)$$

$$t_{irl}^N \ge \frac{d_{rl}^N}{V^{\max}}, \forall i \in I, \forall r \in R, \forall l \in L_r \quad (6)$$

$$q_{ir} \in \mathbb{Z}_+, \forall i \in I, \forall r \in R \quad (7)$$

$$t_{irl}^E \ge 0, \forall i \in I, \forall r \in R, \forall l \in L_r \quad (8)$$

$$t_{irl}^N \ge 0, \forall i \in I, \forall r \in R, \forall l \in L_r \quad (9)$$

$$t_{rl} \ge 0, \forall r \in R, \forall l \in L_r. \quad (10)$$

The objective function minimizes the total costs, which comprises fixed costs, fuel costs, and carbon emission costs across all ship types and routes. Notably, the fuel consumption rate is modeled as a convex and increasing function of sailing speed in the objective function, i.e., the fuel consumption rate within and outside ECAs are equal to $a \cdot (d_{rl}^E / t_{irl}^E)^b$ and $a \cdot (d_{rl}^N / t_{irl}^N)^b$, respectively, where $a > 0$ and $b > 1$ (Wang and Meng 2012, Fagerholt and Psaraftis 2015). Constraints (2) construct the relationship between the rotation time and the total sailing time and port time on a route given the weekly service frequency. Constraints (3) state that the sum of sailing times within and outside the ECAs of a leg is equal to its total sailing time. Constraints (4) limit the total number of ships of each type deployed on all routes. Constraints (5) and (6) ensure that the sailing speeds within and outside ECAs do not exceed the speed limit. Constraints (7) define integer decision variables. The sailing times within and outside ECAs of a leg are defined in Constraints (8) and (9), and the total sailing time of the leg is defined in Constraints (10).

4. Solution method

This MINLP model, featuring several nonlinear parts, intricate interactions, and a sharply increasing number of fleet deployment plans, is highly complex. It is difficult to obtain a high-quality solution for the proposed model using the algorithms directly available in the literature. To address this issue, we first derive key model properties and construct valid inequalities to accelerate the solution process. Then, a piecewise-linear underestimation approximation algorithm and problem-specific characteristics are employed to linearize the nonlinear components. Finally, a tailored algorithm incorporating Benders decomposition and model properties is developed to solve the linearized model, upon which an exact algorithm framework for the original MINLP model is further constructed.

4.1. Model properties

In this section, we derive some model properties and valid inequalities, which are then incorporated into the integrated optimization model. Model properties and valid inequalities play a crucial role in improving the solution method and narrowing the solution space.

4.1.1. Sailing speed inequalities for each leg

Based on the function linking fuel consumption and sailing speed, fuel consumption exhibits convexity with respect to speed, meaning that it increases as speed rises. A strong correlation between speed and fuel prices can also be observed. Given that the maximum sailing speed of type-i ships is $V^{\max}$, we conduct an in-depth analysis of the relationship between optimal sailing speeds within and outside ECAs for type-i ships on leg $l \in L_r$ of route $r \in R$.

Proposition 1. *Consider that only type-i ships are deployed on route $r \in R$. The relationship between the optimal sailing speeds within and outside ECAs on the route is as follows.*

(i) When the maximum optimal sailing speed within and outside ECAs among all legs of the route is less than $V^{\max}$, the ratio of the optimal sailing speeds within ECAs between legs $1, 2, ..., |L_r|$ is $\frac{1}{(c_i^E+c_{ir1}^{car})^{\frac{1}{b+1}}} : \frac{1}{(c_i^E+c_{ir2}^{car})^{\frac{1}{b+1}}} : ... : \frac{1}{(c_i^E+c_{ir|L_r|}^{car})^{\frac{1}{b+1}}}$, and the ratio between the optimal sailing speeds within and outside ECAs on leg $l \in L_r$ is $\left(\frac{c_i^N+c_{irl}^{car}}{c_i^E+c_{irl}^{car}}\right)^{\frac{1}{b+1}}$.

(ii) When there exist sailing legs on the route with an optimal sailing speed equal to $V^{\max}$, the sets of legs with all optimal speeds within ECAs, all optimal speeds outside ECAs, and all optimal speeds within and outside ECAs less than $V^{\max}$ are denoted by L_r', L_r'', and L_r''', respectively. The ratio of optimal sailing speeds within ECAs between the legs of $l_1, l_2, ..., |L_r'| \in L_r'$ is $\frac{1}{(c_i^E+c_{irl_1}^{car})^{\frac{1}{b+1}}} : \frac{1}{(c_i^E+c_{irl_2}^{car})^{\frac{1}{b+1}}} : ... : \frac{1}{(c_i^E+c_{ir|L_r'|}^{car})^{\frac{1}{b+1}}}$, the ratio of optimal sailing speeds outside ECAs between the legs of $l_1, l_2, ..., |L_r''| \in L_r''$ is $\frac{1}{(c_i^N+c_{irl_1}^{car})^{\frac{1}{b+1}}} : \frac{1}{(c_i^N+c_{irl_2}^{car})^{\frac{1}{b+1}}} : ... : \frac{1}{(c_i^N+c_{ir|L_r''|}^{car})^{\frac{1}{b+1}}}$, and the ratio between the optimal sailing speeds within and outside ECAs on leg $l \in L_r'''$ is $\left(\frac{c_i^N+c_{irl}^{car}}{c_i^E+c_{irl}^{car}}\right)^{\frac{1}{b+1}}$.

Proof. See EC.1 in the Electronic Companion. □

According to the analysis in Proposition 1, we define the set of legs covering sailing areas within and outside ECAs on route $r \in R$ as L_r^{EN}. The ratio of the optimal sailing speed within ECAs to that outside ECAs for leg $l \in L_r^{EN}$ of route $r \in R$ is always greater than or equal to $\left(\frac{c_i^N + c_{irl}^{\text{car}}}{c_i^E + c_{irl}^{\text{car}}}\right)^{\frac{1}{b+1}}$. Therefore, we add the following valid inequalities

$$d_{rl}^E t_{irl}^N \geq \left(\frac{c_i^N + c_{irl}^{\text{car}}}{c_i^E + c_{irl}^{\text{car}}}\right)^{\frac{1}{b+1}} \cdot d_{rl}^N t_{irl}^E, \forall i \in I, \forall r \in R, \forall l \in L_r^{EN}. \tag{11}$$

4.1.2. Ship deployment inequalities for each route

When only type-i ships are deployed on route $r \in R$, the minimum number of deployed ships considering the maximum sailing speed of type-i ships is

$$q_r^{\min} = \left\lceil \frac{\sum_{l \in L_r} \frac{d_{rl}^E + d_{rl}^N}{V^{\max}} + T_r}{T} \right\rceil. \tag{12}$$

Define the total cost function of route $r \in R$ with only one type of deployed ship (type-i ships) and the number of deployed ships q_{ir} as

$$f_{ir}(q_{ir}) = c_i^{\text{fix}} q_{ir} + \sum_{l \in L_r} \left[(c_i^E + c_{irl}^{\text{car}}) d_{rl}^E \cdot a \left(\frac{d_{rl}^E}{t_{irl}^E}\right)^b + (c_i^N + c_{irl}^{\text{car}}) d_{rl}^N \cdot a \left(\frac{d_{rl}^N}{t_{irl}^N}\right)^b \right]. \tag{13}$$

We observe the following property of $f_{ir}(q_{ir})$:

Proposition 2. *$f_{ir}(q_{ir})$ with the optimal sailing times within and outside ECAs on all legs of route $r \in R$ is an integrally convex function in q_{ir}.*

Proof. See EC.2 in the Electronic Companion. □

The optimal number of type-i ships deployed on route $r \in R$ is

$$\hat{q}_{ir}^{\text{single}} = \underset{q_{ir} = q_{ir}^{\min}, q_{ir}^{\min}+1, \ldots, Q_i}{\arg\min} f_{ir}(q_{ir}), \tag{14}$$

which can be obtained based on Proposition 2. The following valid inequalities for the number of deployed ships for route r involving only type-i ships under ship type selection plan $p \in P$ are developed:

$$q_r^{\min} \leq \sum_{i \in I} q_{ir} \leq \max_{i \in I} \hat{q}_{ir}^{\text{single}}, \forall r \in R_p^{\text{single}}. \tag{15}$$

When more than one type of ship is deployed on route $r \in R$, the minimum number of deployed ships is still $q_r^{\min}$, while the optimal number of ships deployed on route r, denoted by $\hat{q}_r^{\text{mix}}$, has the following characteristic.

Proposition 3. *The minimum number of deployed ships (denoted by $\hat{q}_r^{mixUB}$) on route r that meets the following two conditions is an upper bound for the optimal number of ships deployed on the route with more than one ship type:*

(i) the number of ships deployed on route r (denoted by q_r^{mixUB}) satisfies $f_r^*(q_r^{mixUB}) - f_r^*(q_r^{mixUB}+1) \le 0$, where $f_r(q_r^{mixUB}) = c^{fixmin} q_r^{mixUB} + \sum_{l\in L_r}\left[(c^{Emax}+c_{rl}^{carmax})d_{rl}^E \cdot a\left(\frac{d_{rl}^E}{t_{1rl}^E}\right)^b + (c^{Nmax}+c_{rl}^{carmax})d_{rl}^N \cdot a\left(\frac{d_{rl}^N}{t_{1rl}^N}\right)^b\right]$, $c^{fixmin} = \min_{i\in I} c_i^{fix}$, $c^{Emax} = \max_{i\in I} c_i^E$, $c^{Nmax} = \max_{i\in I} c_i^N$, $c_{rl}^{carmax} = \max_{i\in I} c_{irl}^{car}$, and $f_r^*(q_r^{mixUB})$ is the minimum value of $f_r(q_r^{mixUB})$.

(ii) the ratio of the optimal sailing time among legs 1, 2, ..., $|L_r|$ for any ship deployment plan $q_{1r}, q_{2r}, ..., q_{|I|r}$ with the total number of deployed ships q_r^{mixUB} (i.e., $q_{1r}+q_{2r}+...+q_{|I|r} = q_r^{mixUB}$) is $\{\frac{q_{1r}}{\sum_{i'\in I'} q_{i'r}}(c_1^N + c_{1r1}^{car})a[(\frac{c_1^E+c_{1r1}^{car}}{c_1^N+c_{1r1}^{car}})^{\frac{1}{b+1}} d_{r1}^E + d_{r1}^N]^{b+1} + \sum_{i\in I'\setminus\{1\}} \frac{q_{ir}}{\sum_{i'\in I'} q_{i'r}}(c_i^N + c_{ir1}^{car})a(d_{r1}^E + d_{r1}^N)^{b+1}\}^{\frac{1}{b+1}} : \{\frac{q_{1r}}{\sum_{i'\in I'} q_{i'r}}(c_1^N + c_{1r2}^{car})a[(\frac{c_1^E+c_{1r2}^{car}}{c_1^N+c_{1r2}^{car}})^{\frac{1}{b+1}} d_{r2}^E + d_{r2}^N]^{b+1} + \sum_{i\in I'\setminus\{1\}} \frac{q_{ir}}{\sum_{i'\in I'} q_{i'r}}(c_i^N + c_{ir2}^{car})a(d_{r2}^E + d_{r2}^N)^{b+1}\}^{\frac{1}{b+1}} : ... : \{\frac{q_{1r}}{\sum_{i'\in I'} q_{i'r}}(c_1^N + c_{1r|L_r|}^{car})a[(\frac{c_1^E+c_{1r|L_r|}^{car}}{c_1^N+c_{1r|L_r|}^{car}})^{\frac{1}{b+1}} d_{r|L_r|}^E + d_{r|L_r|}^N]^{b+1} + \sum_{i\in I'\setminus\{1\}} \frac{q_{ir}}{\sum_{i'\in I'} q_{i'r}}(c_i^N + c_{ir|L_r|}^{car})a(d_{r|L_r|}^E + d_{r|L_r|}^N)^{b+1}\}^{\frac{1}{b+1}}$, where type-1 ships represent traditional ships.

Proof. See EC.3 in the Electronic Companion. □

We calculate the upper bound for $\hat{q}_r^{\text{mix}}$ (denoted by $\hat{q}_r^{\text{mixUB}}$) based on Proposition 3 in Algorithm 1 (see EC.7 in the Electronic Companion). We then have the valid inequalities for the number of different types of ships deployed on route $r \in R$:

$$q_r^{\min} \le \sum_{i\in I} q_{ir} \le \hat{q}_r^{\text{mixUB}}, \forall r \in R_p^{\text{mix}}. \tag{16}$$

4.1.3. Fleet deployment properties for all routes

The availability of multiple types of ships for the shipping company generates numerous feasible fleet deployment plans, which dramatically increases the computation time for solving the proposed model. To improve the computational efficiency, Proposition 4 sheds light on the optimal solutions derived from model [M1] in the context of multiple ship types, offering valuable insights into the optimal fleet deployment decision across service routes.

Proposition 4. *There exists an optimal solution of model [M1] with only $|I|-j$ ($j \ge 1$) service routes each deploying more than one ship type. When there are only $|I|-1$ service routes, each with more than one ship type, each route deploys only two ship types; when there are only $|I|-j$ ($2 \le j \le |I|-j$) service routes, each with more than one ship type, at most $j-1$ routes deploy more than two ship types; when there are only $|I|-j$ ($|I|-j < j \le |I|-1$) service routes, each with more than one ship type, at most $|I|-j$ routes deploy more than two ship types.*

Proof. See EC.4 in the Electronic Companion. □

Based on Proposition 4, large numbers of feasible but non-optimal fleet deployment plans can be excluded, and the feasible domain can be further narrowed by Proposition 5.

Proposition 5. *The fleet deployment plans under ship type selection plan $p \in P$ satisfying any of the following conditions should be excluded.*

(i) Given the type and number of ships deployed on each route $r \in R_p^{mix}$, if the total cost of all routes in R_p^{mix} increases when adding one type-i ship on route $r_1 \in R_p^{mix}$ with the maximum decrease in fuel cost and removing the ship from route $r_2 \in R_p^{mix} \setminus \{r_1\}$ with the minimum increase in fuel cost, i.e., $g_r^*(q_{1r_1}, ..., q_{ir_1} + 1, ..., q_{|I|r_1}) + g_r^*(q_{1r_2}, ..., q_{ir_2} - 1, ..., q_{|I|r_2}) > g_r^*(q_{1r_1}, ..., q_{ir_1}, ..., q_{|I|r_1}) + g_r^*(q_{1r_2}, ..., q_{ir_2}, ..., q_{|I|r_2})$, then the total cost of all routes in R_p^{mix} cannot be reduced by re-deploying q' type-i ships from any route $r_3 \in R_p^{mix} \setminus \{r_1\}$ to $r_1 \in R_p^{mix}$, i.e., $g_r^*(q_{1r_1}, ..., q_{ir_1} + q', ..., q_{|I|r_1}) + g_r^*(q_{1r_3}, ..., q_{ir_3} - q', ..., q_{|I|r_3}) > g_r^*(q_{1r_1}, ..., q_{ir_1}, ..., q_{|I|r_1}) + g_r^*(q_{1r_3}, ..., q_{ir_3}, ..., q_{|I|r_3})$, where $g_r^*(q_{1r}, ..., q_{ir}, ..., q_{|I|r})$ is the minimum cost of route r with ship deployment plan $q_{1r}, ..., q_{ir}, ..., q_{|I|r}$, and $q' \geq 1$ and $q' \in \mathbb{Z}_+$.

(ii) Given the total number of each ship type deployed on the routes of R_p^{single} and R_p^{mix}, if the total cost of all routes in R increases when adding one type-i ship on route $r_1 \in R_p^{mix}$ with the maximum decrease in fuel cost and removing the ship from route $r_2 \in R_p^{single}$ with the minimum increase in fuel cost, i.e., $g_r^*(q_{1r_1}, ..., q_{ir_1} + 1, ..., q_{|I|r_1}) + f_{ir}^*(q_{ir_2} - 1) > g_r^*(q_{1r_1}, ..., q_{ir_1}, ..., q_{|I|r_1}) + f_{ir}^*(q_{ir_2})$, then the total cost of all routes in R cannot be reduced by re-deploying q'' type-i ships from any route $r_3 \in R_p^{single}$ to route $r_1 \in R_p^{mix}$, i.e., $g_r^*(q_{1r_1}, ..., q_{ir_1} + q'', ..., q_{|I|r_1}) + f_{ir}^*(q_{ir_3} - q'') > g_r^*(q_{1r_1}, ..., q_{ir_1}, ..., q_{|I|r_1}) + f_{ir}^*(q_{ir_3})$, where $f_{ir}^*(q_{ir})$ is the minimum cost of route r with ship deployment plan q_{ir}, and $q'' \geq 1$ and $q' \in \mathbb{Z}_+$.

Proof. See EC.5 in the Electronic Companion. □

4.2. Model linearization

Model [M1] is nonlinear because it contains nonlinear terms in the objective function (1), where the nonlinearity is caused by the fuel consumption function and the proportion of each type of deployed ships.

4.2.1. Linearizing fuel consumption functions

We define two nonlinear terms, i.e., fuel consumption functions within and outside ECAs, in the objective function as follows:

$$g_{irl}^E(t_{irl}^E) = d_{rl}^E \cdot a \left(\frac{d_{rl}^E}{t_{irl}^E} \right)^b, \forall i \in I, \forall r \in R, \forall l \in L_r, \tag{17}$$

and

$$g_{irl}^N(t_{irl}^N) = d_{rl}^N \cdot a \left(\frac{d_{rl}^N}{t_{irl}^N} \right)^b, \forall i \in I, \forall r \in R, \forall l \in L_r. \tag{18}$$

Newly added sets

K^E_{irl} Set of piecewise-linear approximating functions of $g^E_{irl}(t^E_{irl})$

K^N_{irl} Set of piecewise-linear approximating functions of $g^N_{irl}(t^N_{irl})$

Newly added parameters

$\text{intercept}^E_{irlk}$ Intercept of the kth piecewise-linear approximating function of $g^E_{irl}(t^E_{irl})$

$\text{intercept}^N_{irlk}$ Intercept of the kth piecewise-linear approximating function of $g^N_{irl}(t^N_{irl})$

slope^E_{irlk} Slope of the kth piecewise-linear approximating function of $g^E_{irl}(t^E_{irl})$

slope^N_{irlk} Slope of the kth piecewise-linear approximating function of $g^N_{irl}(t^N_{irl})$

Newly added variables

g^E_{irl} Fuel consumption within ECAs on leg $l \in L_r$ of route $r \in R$ for type-i ships

g^N_{irl} Fuel consumption outside ECAs on leg $l \in L_r$ of route $r \in R$ for type-i ships

It is not difficult to prove that the functions $g^E_{irl}(t^E_{irl})$ and $g^N_{irl}(t^N_{irl})$ are monotonically decreasing and convex with respect to t^E_{irl} and t^N_{irl}, respectively. Therefore, following the approach outlined by Wang and Meng (2012) and Zhuge et al. (2020), we develop an underestimation approximation scheme to linearize convex functions using some piecewise-linear approximating functions. The fundamental concept involves decomposing a nonlinear function into a combination of several linear parts to achieve an approximate representation of the original function. Referring to Zhuge et al. (2020), the algorithm aims to control the maximum approximation error of fuel consumption within and outside ECAs on legs $l \in L_r$ of route $r \in R$ for type-i ships, denoted as ϵ_{irl}, within the tolerance level. Simultaneously, it seeks to minimize the number of piecewise-linear approximating functions, denoted as $|K^E_{irl}|$ and $|K^N_{irl}|$, where the intercept and slope of the kth piecewise-linear function are denoted as $\text{intercept}^E_{irlk}$ and slope^E_{irlk} for $g^E_{irl}(t^E_{irl})$ and $\text{intercept}^N_{irlk}$ and slope^N_{irlk} for $g^N_{irl}(t^N_{irl})$.

The nonlinear functions $g^E_{irl}(t^E_{irl})$ and $g^N_{irl}(t^N_{irl})$ are then linearized as

$$g^E_{irl} \geq \text{slope}^E_{irlk} t^E_{irl} + \text{intercept}^E_{irlk}, \forall i \in I, \forall r \in R, \forall l \in L_r, \forall k \in K^E_{irl}, \tag{19}$$

$$g^E_{irl} \geq 0, \forall i \in I, \forall r \in R, \forall l \in L_r, \tag{20}$$

and

$$g^N_{irl} \geq \text{slope}^N_{irlk} t^N_{irl} + \text{intercept}^N_{irlk}, \forall i \in I, \forall r \in R, \forall l \in L_r, \forall k \in K^N_{irl}, \tag{21}$$

$$g^N_{irl} \geq 0, \forall i \in I, \forall r \in R, \forall l \in L_r. \tag{22}$$

4.2.2. Linearizing proportion of deployed ships

The nonlinear term in Objective Function (1), arising from the proportion of each deployed ship type (i.e., $\frac{q_{ir}}{\sum_{i' \in I} q_{i'r}}$) on a multi-type route, is further linearized by enumerating the fleet deployment plans. To address the combinatorial complexity of fleet deployment plans, we leverage Proposition 3 to identify upper and lower bounds on the number of ships deployed on each route with multiple ship types, and apply Propositions 4 and 5 to exclude a substantial number of non-optimal deployment plans. The new notation used for each enumerated fleet deployment plan on routes with multiple ship types is defined as follows.

Newly added parameter

$\overline{q}_{ir}$ Given number of type-i ($i \in I$) ships deployed on route $r \in R_p^{\text{mix}}$

Newly added variable

x_{ir} Binary variable, equal to one if type-i ($i \in I$) ships are deployed on route $r \in R$, and zero otherwise

The mixed-integer linear programming (MILP) model for each enumeration is then formulated.

$$\begin{aligned}[\text{M2}]\ \min & \sum_{i \in I} \sum_{r \in R_p^{\text{mix}}} c_i^{\text{fix}} \overline{q}_{ir} + \sum_{i \in I} \sum_{r \in R_p^{\text{single}}} c_i^{\text{fix}} q_{ir} + \sum_{r \in R_p^{\text{mix}}} \sum_{i \in I} \frac{\overline{q}_{ir}}{\sum_{i' \in I} \overline{q}_{i'r}} \sum_{l \in L_r} [(c_i^E + c_{irl}^{\text{car}}) g_{irl}^E \\ & + (c_i^N + c_{irl}^{\text{car}}) g_{irl}^N] + \sum_{r \in R_p^{\text{single}}} \sum_{i \in I} \sum_{l \in L_r} \left[(c_i^E + c_{irl}^{\text{car}}) g_{irl}^E + (c_i^N + c_{irl}^{\text{car}}) g_{irl}^N\right] \end{aligned} \tag{23}$$

subject to Constraints (2)–(11), (15), (20), (22), and

$$q_{ir} \le \hat{q}_{ir}^{\text{single}} \cdot x_{ir}, \forall i \in I, \forall r \in R_p^{\text{single}} \tag{24}$$

$$\sum_{i \in I} x_{ir} = 1, \forall r \in R_p^{\text{single}} \tag{25}$$

$$g_{irl}^E \ge \text{slope}_{irlk}^E t_{irl}^E + \text{intercept}_{irlk}^E - M_1(1 - x_{ir}), \forall i \in I, \forall r \in R, \forall l \in L_r, \forall k \in K_{irl}^E \tag{26}$$

$$g_{irl}^N \ge \text{slope}_{irlk}^N t_{irl}^N + \text{intercept}_{irlk}^N - M_2(1 - x_{ir}), \forall i \in I, \forall r \in R, \forall l \in L_r, \forall k \in K_{irl}^N \tag{27}$$

$$x_{ir} \in \{0, 1\}, \forall i \in I, \forall r \in R, \tag{28}$$

where $M_1 = \max\{\text{intercept}_{irlk}^E, \forall i \in I, \forall r \in R, \forall l \in L_r, \forall k \in K_{irl}^E\}$ and $M_2 = \max\{\text{intercept}_{irlk}^N, \forall i \in I, \forall r \in R, \forall l \in L_r, \forall k \in K_{irl}^N\}$.

The optimal objective value of model [M2] is denoted as $\text{LB}_{\text{[M1]}}$, and the optimal value of model [M1] is denoted as $\text{Opt}_{\text{[M1]}}$, where $\text{LB}_{\text{[M1]}}$ serves as a lower bound of $\text{Opt}_{\text{[M1]}}$, because we use a piecewise-linear underestimation approximation algorithm to linearize the nonlinear terms of model

[M1]. The fuel consumption of each leg in model [M2] may be underestimated, and thus the optimal solution of model [M2] (recorded as q^*_{ir}, t^*_{rl}, t^{E*}_{irl}, and t^{N*}_{irl}) is feasible but may not be optimal for model [M1]. We substitute q^*_{ir}, t^*_{rl}, t^{E*}_{irl}, and t^{N*}_{irl} into model [M1] and obtain its objective value, denoted as $\text{UB}_{[\text{M1}]}$, serving as an upper bound of $\text{Opt}_{[\text{M1}]}$. Therefore, the maximum approximation error for model [M2] is

$$\epsilon_{[\text{M1}]} = \sum_{r\in R}\sum_{i\in I}\frac{q^*_{ir}}{\sum_{i'\in I} q^*_{i'r}}\sum_{l\in L_r}[(c^E_i + c^{\text{car}}_{irl})\epsilon_{irl} + (c^N_i + c^{\text{car}}_{irl})\epsilon_{irl}]. \tag{29}$$

As such, we conclude that

$$\text{LB}_{[\text{M1}]} \le \text{Opt}_{[\text{M1}]} \le \text{UB}_{[\text{M1}]} \le \text{LB}_{[\text{M1}]} + \epsilon_{[\text{M1}]}. \tag{30}$$

4.3. Benders decomposition and property-based exact algorithm

Benders decomposition is widely used to solve large-scale optimization problems (Chen et al. 2018a). By decomposing the original problem into a master problem and one or more subproblems, Benders decomposition effectively reduces computational complexity and enhances solution efficiency. Considering the complexity of our research problem, we design a tailored Benders decomposition algorithm that consists of an iterative process of solving a master problem and a series of subproblems, where a tailored cut pool is designed to improve the solution efficiency and the model properties derived in Section 4.1 (i.e., Propositions 1, 2, 3, 4, and 5) are used to narrow the solution space. Based on the results of this tailored algorithm, we develop an exact solution framework for the original MINLP model that is suitable for large-scale shipping networks.

4.3.1. Subproblem design

We decompose the MILP model [M2] into an integer master problem and a linear subproblem. Once the relevant variables of the master problem are fixed, the corresponding subproblem becomes a linear programming problem with only continuous variables. Let $\overline{q}_{ir}$ and $\overline{x}_{ir}$ denote the fixed values of q_{ir} and x_{ir}, respectively. In the subproblem, we have $\overline{q} := \{\overline{q}_{ir} \mid i \in I, r \in R\}$ and $\overline{x} := \{\overline{x}_{ir} \mid i \in I, r \in R\}$ satisfying Constraints (4), (7), (15), (24)–(25), and (28). Therefore, based on Proposition 1, the subproblem [M2-SP] is:

$$\begin{aligned}[\text{M2-SP}]\ \min\ & \sum_{r\in R^{\text{mix}}_p}\sum_{i\in I}\frac{\overline{q}_{ir}}{\sum_{i'\in I}\overline{q}_{i'r}}\sum_{l\in L_r}\left[(c^E_i + c^{\text{car}}_{irl})g^E_{irl} + (c^N_i + c^{\text{car}}_{irl})g^N_{irl}\right] \\ & + \sum_{r\in R^{\text{single}}_p}\sum_{i\in I}\sum_{l\in L_r}\left[(c^E_i + c^{\text{car}}_{irl})g^E_{irl} + (c^N_i + c^{\text{car}}_{irl})g^N_{irl}\right]\end{aligned} \tag{31}$$

subject to Constraints (2)–(3), (5)–(6), (8)–(11), (20), (22), and (26)–(27).

We define $\delta=\{\delta_r \mid r\in R\}$, $\alpha=\{\alpha_{irl} \mid i\in I,\ r\in R,\ l\in L_r\}$, $\gamma=\{\gamma_{irl} \mid i\in I,\ r\in R,\ l\in L_r\}$, $\tau=\{\tau_{irl} \mid i\in I,\ r\in R,\ l\in L_r\}$, $\beta=\{\beta_{irl} \mid i\in I,\ r\in R,\ l\in L_r\}$, $\lambda=\{\lambda^k_{irl} \mid i\in I,\ r\in R,\ l\in L_r,\ k=1,2,\ldots,K^E_{irl}\}$, and $\eta=\{\eta^k_{irl} \mid i\in I,\ r\in R,\ l\in L_r,\ k=1,2,\ldots,K^N_{irl}\}$ as the dual variables associated with Constraints (2), (3), (5), (6), (11), (26), and (27), respectively. The dual model of the primal subproblem [M2-DSP] is written as

[M2-DSP]

$$\max \sum_{r\in R}\sum_{i\in I}\sum_{l\in L_r}\sum_{k=1}^{K^E_{irl}}[\text{intercept}^E_{irlk}-M_1(1-\overline{x}_{ir})]\lambda^k_{irl}+\sum_{r\in R}\sum_{i\in I}\sum_{l\in L_r}\frac{d^E_{rl}}{V^{\max}}\gamma_{irl}+\sum_{r\in R}\sum_{i\in I}\sum_{l\in L_r}\frac{d^N_{rl}}{V^{\max}}\tau_{irl}$$
$$+\sum_{r\in R}\sum_{i\in I}\sum_{l\in L_r}\sum_{k=1}^{K^N_{irl}}[\text{intercept}^N_{irlk}-M_2(1-\overline{x}_{ir})]\eta^k_{irl}+\sum_{r\in R}\ (\sum_{i\in I}\overline{q}_{ir}T-T_r)\delta_r \tag{32}$$

subject to

$$\delta_r+\alpha_{irl}\le 0,\forall i\in I,\forall r\in R,\forall l\in Lr \tag{33}$$

$$\gamma_{irl}-\alpha_{irl}-\left(\frac{c^N_i+c^{\text{car}}_{irl}}{c^E_i+c^{\text{car}}_{irl}}\right)^{\frac{1}{b+1}}d^N_{rl}\beta_{irl}-\sum_{k=1}^{K^E_{irl}}\text{slope}^E_{irlk}\lambda^k_{irl}\le 0,\forall i\in I,\forall r\in R,\forall l\in Lr \tag{34}$$

$$\tau_{irl}-\alpha_{irl}+d^E_{rl}\beta_{irl}-\sum_{k=1}^{K^N_{irl}}\text{slope}^N_{irlk}\eta^k_{irl}\le 0,\forall i\in I,\forall r\in R,\forall l\in Lr \tag{35}$$

$$\sum_{k=1}^{K^E_{irl}}\lambda^k_{irl}\le\frac{\overline{q}_{ir}}{\sum_{i'\in I}\overline{q}_{i'r}}\left(c^E_i+c^{\text{car}}_{irl}\right),\forall i\in I,\forall r\in R^{\text{mix}}_p,\forall l\in Lr \tag{36}$$

$$\sum_{k=1}^{K^E_{irl}}\lambda^k_{irl}\le\left(c^E_i+c^{\text{car}}_{irl}\right),\forall i\in I,\forall r\in R^{\text{single}}_p,\forall l\in Lr \tag{37}$$

$$\sum_{k=1}^{K^N_{irl}}\eta^k_{irl}\le\frac{\overline{q}_{ir}}{\sum_{i'\in I}\overline{q}_{i'r}}\left(c^N_i+c^{\text{car}}_{irl}\right),\forall i\in I,\forall r\in R^{\text{mix}}_p,\forall l\in Lr \tag{38}$$

$$\sum_{k=1}^{K^N_{irl}}\eta^k_{irl}\le\left(c^N_i+c^{\text{car}}_{irl}\right),\forall i\in I,\forall r\in R^{\text{single}}_p,\forall l\in Lr \tag{39}$$

$$\beta,\lambda,\eta,\gamma,\tau\ge 0 \tag{40}$$

$$\delta,\alpha\in\mathbb{R}, \tag{41}$$

where $\mathbb{R}$ is the set of real numbers. We obtain the following proposition for the subproblem and its dual model, meaning that no feasibility cuts will be added to the master problem [M2-MP].

Proposition 6. *The feasibility and boundedness of [M2-SP] and [M2-DSP] are ensured.*

Proof. See EC.6 in the Electronic Companion. □

Proposition 6 shows that, according to the constraints outlined in model [M2-SP], any feasible solution derived from the primal subproblem must inherently be bounded. Consequently, this condition ensures that the dual of the primal subproblem maintains feasibility and boundedness at all times. Hence, only optimality cuts will be incorporated into the master problem.

4.3.2. Master problem with tailored cut pool

A core feature of the tailored Benders decomposition algorithm lies in the construction and management of the cut pool, which incrementally approximates the objective functions of the subproblems and steers the master problem toward the global optimum. To ensure both accuracy and computational efficiency in the proposed algorithm, we develop a systematic cut pool construction and management strategy consisting of three components: a route-driven optimality cut formulation that exploits the problem's separable structure and captures route-level decision sensitivities; a speed-guided adaptive cut generation scheme that dynamically refines the approximation based on operational characteristics; and a dynamic cut reduction mechanism that controls the cut pool size by pruning inactive or weakly relevant cuts while preserving essential information for convergence. The generated Benders cuts are subsequently integrated into the master problem formulation, enabling its progressive refinement toward global optimality through iterative updates.

(1) Route-driven optimality cut

Once the fleet deployment decisions are fixed in the master problem, the subproblems associated with different routes become independent. To better exploit the separable structure of the proposed model, we formulate Benders optimality cuts into a route-driven form. Specifically, instead of constructing a single global cut representing the entire network, one optimality cut is generated for each route and aggregated into the master problem through route-level auxiliary variables θ_r, $r \in R_p^{\text{single}}$. Let $(\overline{\delta}_r, \overline{\alpha}_r, \overline{\beta}_r, \overline{\lambda}_r, \overline{\eta}_r, \overline{\gamma}_r, \overline{\tau}_r)$ denote the optimal solution of the dual subproblem [M2-DSP] for each route r. The corresponding route-driven optimality cut for route r is then formulated as follows:

$$\theta_r \geq \sum_{i\in I}\sum_{l\in L_r}\sum_{k=1}^{K^E_{irl}}[\text{intercept}^E_{irlk} - M_1(1-x_{ir})]\overline{\lambda}^k_{irl} + \sum_{i\in I}\sum_{l\in L_r}\frac{d^E_{rl}}{V^{\max}}\overline{\gamma}_{irl} + \sum_{i\in I}\sum_{l\in L_r}\frac{d^N_{rl}}{V^{\max}}\overline{\tau}_{irl}$$
$$+\sum_{i\in I}\sum_{l\in L_r}\sum_{k=1}^{K^N_{irl}}[\text{intercept}^N_{irlk} - M_2(1-x_{ir})]\overline{\eta}^k_{irl} + (\sum_{i\in I} q_{ir}T - T_r)\overline{\delta}_r, \forall(\overline{\delta}_r, \overline{\alpha}_r, \overline{\beta}_r, \overline{\lambda}_r, \overline{\eta}_r, \overline{\gamma}_r, \overline{\tau}_r) \in \Xi_r, \quad (42)$$

where Ξ_r represents the set of extreme points of the feasible region of [M2-DSP] for route $r \in R_p^{\text{single}}$. The route-driven cut generation allows each subproblem to construct a locally tighter linear approximation of its optimal value, thereby improving the overall accuracy of the lower bound. It also enables parallel computation of subproblems and makes full use of route-specific sensitivity information, such as heterogeneous carbon emission costs and ECA configurations, during the cut generation process. Compared with conventional aggregated cuts, the proposed route-driven approach significantly enhances convergence stability and computational efficiency.

(2) Speed-guided adaptive cut

We further enhance the Benders decomposition algorithm by generating adaptive cuts, guided by the sailing speed characteristics identified in Proposition 1 and the integrally convex property of the cost function for routes deploying a single ship type (Proposition 2). For each route operated by a single ship type $i \in I$, the generation of adaptive cuts depends on the total number of available ships Q_i and the current ship deployment $\sum_{r\in R} q_{ir}$. (i) When $Q_i - \sum_{r\in R} q_{ir} = 0$, we adjust the deployment plan on routes with the most extreme sailing speeds: select the top $m\%$ ($m \leq 30$) of routes with the highest optimal sailing speeds, collected in R_{ip}^{top}, and increase the number of ships on each such route $r \in R_{ip}^{\text{top}}$ to $\min\{\overline{q}_{ir}+1, \hat{q}_{ir}^{\text{single}}\}$; select the bottom $m\%$ of routes with the lowest optimal sailing speeds, collected in R_{ip}^{bot}, and reduce the number of ships on each such route $r \in R_{ip}^{\text{bot}}$ to $\max\{\overline{q}_{ir}-1, q_r^{\min}\}$. (ii) When $Q_i - \sum_{r\in R} q_{ir} > 0$, we further increase deployment on high-speed routes by selecting $\min\{2m \cdot \sum_{r\in R} q_{ir}, Q_i - \sum_{r\in R} q_{ir}\}$ routes with the highest optimal sailing speeds, collected in R_{ip}^{top}, and adjusting each route $r \in R_{ip}^{\text{top}}$ to $\min\{\overline{q}_{ir}+1, \hat{q}_{ir}^{\text{single}}\}$. The adjusted ship number for route $r \in R_{ip}^{\text{top}} \cup R_{ip}^{\text{bot}}$ is denoted by $\tilde{q}_{ir}$:

$$\tilde{q}_{ir} = \begin{cases} \min\{\overline{q}_{ir}+1, \hat{q}_{ir}^{\text{single}}\}, & r \in R_{ip}^{\text{top}}, \\ \max\{\overline{q}_{ir}-1, q_r^{\min}\}, & r \in R_{ip}^{\text{bot}}. \end{cases} \tag{43}$$

After the deployment plan is adjusted, we replace the original ship deployment variable $\overline{q}_{ir}$ in the dual subproblem [M2-DSP] with the updated value $\tilde{q}_{ir}$ and re-solve the dual subproblem to obtain new solutions. Based on these solutions, the adaptive cuts are subsequently generated. Let $(\tilde{\delta}_r, \tilde{\alpha}_r, \tilde{\beta}_r, \tilde{\lambda}_r, \tilde{\eta}_r, \tilde{\gamma}_r, \tilde{\tau}_r)$ denote the optimal solution of the dual subproblem for each route $r \in R_p^{\text{top}} \cup R_p^{\text{bot}}$. The corresponding adaptive cuts are then generated as:

$$\begin{aligned} \theta_r \geq & \sum_{i\in I}\sum_{l\in L_r}\sum_{k=1}^{K_{irl}^E} [\text{intercept}_{irlk}^E - M_1(1-x_{ir})]\tilde{\lambda}_{irl}^k + \sum_{i\in I}\sum_{l\in L_r} \frac{d_{rl}^E}{V^{\max}}\tilde{\gamma}_{irl} + \sum_{i\in I}\sum_{l\in L_r} \frac{d_{rl}^N}{V^{\max}}\tilde{\tau}_{irl} \\ & + \sum_{i\in I}\sum_{l\in L_r}\sum_{k=1}^{K_{irl}^N} [\text{intercept}_{irlk}^N - M_2(1-x_{ir})]\tilde{\eta}_{irl}^k + \ (\sum_{i\in I} q_{ir}T - T_r)\tilde{\delta}_r, \forall (\tilde{\delta}_r, \tilde{\alpha}_r, \tilde{\beta}_r, \tilde{\lambda}_r, \tilde{\eta}_r, \tilde{\gamma}_r, \tilde{\tau}_r) \in \Pi_r, \end{aligned} \tag{44}$$

where Π_r represents the set of extreme points of the feasible region of [M2-DSP] for route $r \in R_p^{\text{top}} \cup R_p^{\text{bot}}$. The adaptive mechanism dynamically adjusts the generation of Benders cuts according

to the operational characteristics of route-level speed decisions. By emphasizing routes with the most significant sensitivity in sailing speed, the algorithm focuses computational effort on promising regions of the solution space, thereby improving convergence efficiency and solution quality.

(3) Dynamic cut reduction mechanism

Due to the introduction of the route-driven optimality cuts and the speed-guided adaptive cuts, the total number of Benders cuts can increase rapidly, potentially leading to an excessive cut pool and deteriorated computational performance of the master problem. To address this issue, we introduce a dynamic cut reduction (DCR) mechanism to control the cut pool size and maintain computational efficiency.

When the total number of Benders cuts exceeds a predefined threshold N ($N \geq 5|R|$), we selectively remove cuts that are temporarily irrelevant to the current master problem. For each route $r \in R$, we identify whether its optimal ship type and deployment number have remained unchanged over the most recent n' ($n' \geq 3$) iterations. If this condition is satisfied, we regard route r as locally stable and examine the relevance of its associated Benders cuts. Among the cuts contained in Ξ_r and Π_r, those that do not affect the current optimal solution (denoted by $\overline{q}_{ir}$, $\overline{x}_{ir}$, and $\overline{\theta}_r$) are temporarily removed, yielding updated extreme point sets Ξ'_r and Π'_r. Specifically, a cut is removed only if, after its removal, when all other routes are fixed at their current solutions, the equality $\sum_{i\in I} c_i^{\text{fix}}\overline{q}_{ir} + \overline{\theta}_r = \min \sum_{i\in I} c_i^{\text{fix}} q_{ir} + \theta_r$ still holds subject to Constraints (7), (15), (24), (25), (28), (42), and (44) under the reduced extreme point sets Ξ'_r and Π'_r. All removed cuts of route r are stored in a separate set Ω_r. Note that the removal is only temporary. A removed cut will be reactivated if its corresponding ship deployment plan—defined by the ship type and number deployed on route r—is chosen in subsequent master problem iterations. More precisely, when the master problem selects a ship deployment plan that matches the structural pattern associated with a cut stored in Ω_r, the corresponding cut is immediately re-added to the active extreme point set Ξ'_r or Π'_r. This mechanism prevents unnecessary accumulation of redundant cuts while ensuring that potentially valuable information can be efficiently retrieved when relevant structural patterns recur. As a result, the proposed DCR mechanism achieves a balance between computational efficiency and solution quality.

(4) Master problem formulation

Following the construction of the tailored cut pool, we formulate the master problem as

$$[\text{M2-MP}] \min \sum_{i\in I}\sum_{r\in R} c_i^{\text{fix}} q_{ir} + \sum_{r\in R} \theta_r \tag{45}$$

subject to Constraints (4), (7), (15), (24), (25), (28), (42), and (44). The proposed tailored Benders decomposition algorithm guarantees finite convergence because the master problem is iteratively

strengthened by valid optimality cuts derived from the solutions of the dual subproblems. As the number of iterations increases, the lower and upper bounds converge monotonically, leading to an optimal solution when the gap is equal to zero.

To further enhance the computational efficiency of the model, we selectively prune fleet deployment plans by leveraging Propositions 3, 4, and 5, which are used as input for the subsequent solution procedure. We then summarize the complete framework of the Benders decomposition and the property-based algorithm in Algorithm 2 (see EC.8 in the Electronic Companion), where Proposition 2 and Proposition 1 are employed to reduce the feasible regions of the master problem and the subproblem, respectively.

4.3.3. Exact algorithm framework for the MINLP model

To address the potential accuracy loss introduced by piecewise linearization, we further derive the optimal solution of the original MINLP model using the results obtained from the tailored Benders decomposition algorithm. As shown in Eq. (30), the minimum total cost of the linearized model is always lower than that of the MINLP model [M1] for a given fleet deployment plan on routes with multiple ship types. Leveraging this property, we establish the following corollary.

Corollary 1. *If the optimal objective value of the linearized model [M2] under a given fleet deployment plan on routes with multiple ship types is greater than the optimal objective value of the MINLP model [M1] under another such plan, the former plan cannot be globally optimal.*

By combining this corollary with the propositions on optimal sailing speed and sailing time, we develop an enhanced exact algorithm to obtain the optimal solution of the MINLP model [M1], which consists of three main steps (see Algorithm 3 in EC.9 of the Electronic Companion). Step 1 identifies the optimal fleet deployment plan and corresponding decisions that yield the minimum total cost in the linearized model [M2] among all candidate plans. Step 2 substitutes the optimal deployment decisions obtained in Step 1 into the MINLP model, analytically determines the optimal sailing speeds according to Propositions 1 and 3(ii), and calculates the corresponding total cost. The global minimum cost of the MINLP model is then updated if a lower value is found. Step 3 updates the candidate plans by removing non-optimal ones, i.e., for each plan, the minimum total costs obtained from the MINLP and linearized models are compared, and any plan whose linearized cost is no lower than the current best nonlinear cost is removed. The above three steps are iteratively executed until no candidate plans remain.

5. Numerical experiments

In this section, we perform extensive numerical experiments to evaluate the effectiveness of the proposed model and the exact algorithm based on Benders decomposition and model properties. The experiments are conducted on a personal computer (Intel Core i7, 2.5GHz; 8GB RAM), with the solution process implemented in C# (VS 2022) using CPLEX 20.1.

5.1. Experimental settings

The experimental data are derived from real-world sources. Four experimental groups are set up, consisting of 5, 10, 30, and 50 routes, with an average of eight ports of call per route. Each group comprises five test instances. All ECAs designated by the IMO are considered. The time spent at each port of call on the routes follows a uniform distribution between 12 and 60 hours (Qi and Song 2012). The container ships operated by the shipping company are assumed to have a capacity of 18,000 TEU and a maximum speed of 23 knots (Seatrade-ShipTech-Middle-East 2019). Three types of ships are involved, i.e., traditional ships (type-1), scrubber-equipped ships (type-2), and LNG-powered ships (type-3). We refer to MI-News-Network (2017), Gu and Wallace (2017), and Seatrade-ShipTech-Middle-East (2019) for the fixed costs of type-1, type-2, and type-3 ships, which are set at 271,700 US$ per week, 283,500 US$ per week, and 308,800 US$ per week, respectively. The prices of VLSFO, MGO, HSFO, and LNG are set based on the global average fuel prices in 2024 (Ship and Bunker 2024). Recall that all fuel prices have been adjusted to an energy-equivalent basis, with VLSFO serving as the reference. For ships using HSFO, VLSFO, MGO, or LNG as fuel, the conversion factors between fuel consumption per unit distance and sailing speed are denoted as a and b, where a takes the value of 7.81×10^{-4} and b takes the value of 2 (MI-News-Network 2017). The carbon emission cost is set within a range of 51 to 185 US$/ton (Rennert et al. 2022).

5.2. Performance of the proposed exact algorithm

We analyze four groups of test instances with 5, 10, 30, and 50 service routes to validate the efficiency of the proposed exact algorithm. We implement a CPLEX-based benchmark algorithm for comparison: the linearized model is solved using the CPLEX solver and, in combination with Algorithm 3, yields the exact solution of the MINLP model [M1]. The computational results for all instances are reported in Table 2. As shown, the optimal objective values obtained by the proposed exact algorithm are identical to those produced by the CPLEX-based algorithm, confirming its solution quality. Regarding computational efficiency, the proposed algorithm is more than 90 times faster than the CPLEX-based algorithm for the smallest instances. As the instance size increases, the CPLEX-based algorithm fails to find the optimal solution within the three-hour time limit, whereas the proposed algorithm consistently solves all instances to optimality within a reasonable time, i.e., two hours. Overall, these results demonstrate that the proposed exact algorithm not only guarantees optimality but also significantly enhances scalability and computational efficiency.

5.3. Impact of fuel price changes on fleet deployment

This section examines how changes in fuel prices influence the types and number of ships deployed on routes. We analyze a case with 10 routes and three ship types, each type initially configured with 30 ships. Baseline fuel prices are set as follows: VLSFO at 650 US$/ton, with energy-equivalent

Table 2 Comparison between the proposed exact algorithm and the CPLEX-based benchmark algorithm

Instances	Proposed exact algorithm		CPLEX-based benchmark algorithm		Gap
	Obj_B	CPU time (s)	Obj_C	CPU time (s)	
5-1	13,489,566	106	13,489,566	9,962	0
5-2	12,367,710	102	12,367,710	9,735	0
5-3	13,727,060	86	13,727,060	9,048	0
5-4	12,786,435	98	12,786,435	9,461	0
5-5	12,290,281	93	12,290,281	9,175	0
10-1	26,539,595	556	–	–	–
10-2	26,657,145	497	–	–	–
10-3	26,174,011	603	–	–	–
10-4	27,471,281	576	–	–	–
10-5	25,439,118	484	–	–	–
30-1	78,159,160	2,954	–	–	–
30-2	77,568,748	3,482	–	–	–
30-3	79,739,116	3,187	–	–	–
30-4	78,583,329	3,560	–	–	–
30-5	80,663,949	2,971	–	–	–
50-1	125,737,554	6,504	–	–	–
50-2	133,563,015	6,800	–	–	–
50-3	128,454,691	6,636	–	–	–
50-4	126,860,357	7,027	–	–	–
50-5	130,451,745	7,180	–	–	–

Notes:

(i) Instance "5-1" refers to the first instance for the group of five routes.
(ii) "Obj_B" and "Obj_C" denotes the optimal objective values for the MINLP model [M1] obtained by the proposed exact algorithm and the CPLEX-based benchmark algorithm, respectively.
(iii) "Gap" is calculated as (Obj_B - Obj_C)/Obj_C.

unit prices of MGO, HSFO, and LNG adjusted to 800 US$, 500 US$, and 480 US$, respectively. We assess the impact of price fluctuations of ±50, ±100, and ±150 US$/ton on ship type selection and the number of ships deployed on routes.

As shown in Table 3, under the baseline prices, 30 type-1 ships, 30 type-2 ships, and 8 type-3 ships are deployed across the 10 routes. When the price of MGO/VLSFO decreases by 50, 100, or 150 US$/ton or increases by 50 or 100 US$/ton from the baseline, the ship deployment plan on each route remains unchanged. When the price of MGO/VLSFO rises by 150 US$/ton, the number

of type-1 ships decreases to 7, while the number of type-3 ships increases to 30. This trend suggests that as MGO and VLSFO prices rise significantly, the increasing fuel costs for traditional ships drive the shipping company to prefer type-3 ships, which have lower total costs (comprising fixed costs, fuel costs, and carbon emission costs). The number of type-2 ships remains stable, with all type-2 ships deployed across all price changes, due to their lower overall costs.

Table 4 shows that as the price of HSFO decreases significantly, the ship deployment plans for several routes change, but the numbers of deployed type-1 and type-2 ships remain unchanged. However, with a large increase in HSFO price, both the ship deployment plans and the number of deployed ships for each type are affected—specifically, the numbers of type-1 and type-2 ships slightly decrease, while the number of type-3 ships slightly increases. These changes are primarily driven by the cost efficiency of type-2 ships in terms of both fuel and fixed costs, allowing them to remain competitive within a certain price range.

According to Table 5, when the price of LNG increases or slightly decreases, the ship deployment plans remain unchanged. However, when the price of LNG decreases by 100 US$/ton or more, the number of type-3 ships gradually increases, while the number of type-1 ships gradually decreases, and the number of type-2 ships remains unaffected. This trend indicates that as the price of LNG decreases, shipping companies are more inclined to select LNG-powered ships. The lower fuel cost of type-3 ships enhances their economic and competitive advantages, leading to a gradual replacement of type-1 ships.

Table 3 Impact of MGO/VLSFO price changes on the types and number of deployed ships

Routes \ Unit price change	-150	-100	-50	0	50	100	150
1	(7,1,1)	(7,1,1)	(7,1,1)	(7,1,1)	(7,1,1)	(7,1,1)	(7,1,1)
2	(0,6,0)	(0,6,0)	(0,6,0)	(0,6,0)	(0,6,0)	(0,6,0)	(0,0,6)
3	(0,0,7)	(0,0,7)	(0,0,7)	(0,0,7)	(0,0,7)	(0,0,7)	(0,0,7)
4	(7,0,0)	(7,0,0)	(7,0,0)	(7,0,0)	(7,0,0)	(7,0,0)	(0,7,0)
5	(9,0,0)	(9,0,0)	(9,0,0)	(9,0,0)	(9,0,0)	(9,0,0)	(0,9,0)
6	(0,6,0)	(0,6,0)	(0,6,0)	(0,6,0)	(0,6,0)	(0,6,0)	(0,0,6)
7	(0,5,0)	(0,5,0)	(0,5,0)	(0,5,0)	(0,5,0)	(0,5,0)	(0,0,5)
8	(0,6,0)	(0,6,0)	(0,6,0)	(0,6,0)	(0,6,0)	(0,6,0)	(0,6,0)
9	(7,0,0)	(7,0,0)	(7,0,0)	(7,0,0)	(7,0,0)	(7,0,0)	(0,7,0)
10	(0,6,0)	(0,6,0)	(0,6,0)	(0,6,0)	(0,6,0)	(0,6,0)	(0,0,5)

Note: (a,b,c) represents (number of type-1 ships, number of type-2 ships, number of type-3 ships).

Table 4 Impact of HSFO price changes on the types and number of deployed ships

Routes \ Unit price change	-150	-100	-50	0	50	100	150
1	(7,1,1)	(7,1,1)	(7,1,1)	(7,1,1)	(7,1,1)	(7,1,1)	(7,1,1)
2	(0,6,0)	(0,6,0)	(0,6,0)	(0,6,0)	(0,6,0)	(0,7,0)	(0,7,0)
3	(0,7,0)	(0,7,0)	(0,0,7)	(0,0,7)	(0,0,7)	(0,7,0)	(0,7,0)
4	(7,0,0)	(7,0,0)	(7,0,0)	(7,0,0)	(7,0,0)	(0,7,0)	(0,7,0)
5	(9,0,0)	(9,0,0)	(9,0,0)	(9,0,0)	(9,0,0)	(9,0,0)	(9,0,0)
6	(0,6,0)	(0,6,0)	(0,6,0)	(0,6,0)	(0,6,0)	(6,0,0)	(6,0,0)
7	(0,0,5)	(0,0,5)	(0,5,0)	(0,5,0)	(0,5,0)	(0,0,5)	(0,0,5)
8	(0,5,0)	(0,5,0)	(0,6,0)	(0,6,0)	(0,6,0)	(0,6,0)	(0,6,0)
9	(7,0,0)	(7,0,0)	(7,0,0)	(7,0,0)	(7,0,0)	(7,0,0)	(7,0,0)
10	(0,5,0)	(0,5,0)	(0,6,0)	(0,6,0)	(0,6,0)	(0,0,5)	(0,0,5)

Table 5 Impact of LNG price changes on the types and number of deployed ships

Routes \ Unit price change	-150	-100	-50	0	50	100	150
1	(7,1,1)	(7,1,1)	(7,1,1)	(7,1,1)	(7,1,1)	(7,1,1)	(7,1,1)
2	(0,0,6)	(0,7,0)	(0,6,0)	(0,6,0)	(0,6,0)	(0,6,0)	(0,6,0)
3	(0,0,7)	(0,7,0)	(0,0,7)	(0,0,7)	(0,0,7)	(0,0,7)	(0,0,7)
4	(0,7,0)	(7,0,0)	(7,0,0)	(7,0,0)	(7,0,0)	(7,0,0)	(7,0,0)
5	(0,9,0)	(0,9,0)	(9,0,0)	(9,0,0)	(9,0,0)	(9,0,0)	(9,0,0)
6	(0,0,6)	(0,6,0)	(0,6,0)	(0,6,0)	(0,6,0)	(0,6,0)	(0,6,0)
7	(0,0,5)	(0,0,5)	(0,5,0)	(0,5,0)	(0,5,0)	(0,5,0)	(0,5,0)
8	(0,0,5)	(0,0,5)	(0,6,0)	(0,6,0)	(0,6,0)	(0,6,0)	(0,6,0)
9	(0,7,0)	(7,0,0)	(7,0,0)	(7,0,0)	(7,0,0)	(7,0,0)	(7,0,0)
10	(0,6,0)	(0,0,5)	(0,6,0)	(0,6,0)	(0,6,0)	(0,6,0)	(0,6,0)

5.4. Impact of fuel price changes on sailing time

In this section, we discuss how fuel price fluctuations affect the sailing time of three types of ships deployed on the same route. Focusing on a route with eight legs and three ship types, we assess the impact of MGO/VLSFO, HSFO, and LNG price variations on the sailing time of each leg. The baseline sailing time for each type of ship on each leg is set as the optimal sailing time when only one ship type is deployed, maintaining the same total number of deployed ships. Figs. 2, 3,

and 4 present the average deviation in sailing time across all legs under different fuel price changes relative to their baselines.

As shown in Fig. 2, as the price of MGO/VLSFO rises, the average sailing time gap for type-1 ships across the eight legs gradually decreases and approaches zero, while the gaps for type-2 and type-3 ships continue to widen. The reason is that different ship types operating on the same route must synchronize their schedules, preventing them from individually optimizing their speeds. As MGO/VLSFO prices increase, the coordinated schedule aligns more closely with the optimal sailing time for type-1 ships, helping to minimize total fuel costs. In Figs. 3 and 4, when the HSFO or LNG price increases, the sailing time gaps for type-2 and type-3 ships continue to decrease and the gap for type-1 ships steadily increases. The main reason is that type-2 and type-3 ships have similar optimal schedules, causing the schedule to shift toward their optimal sailing times with the increase in HSFO or LNG price, whereas type-1 ships differ significantly.

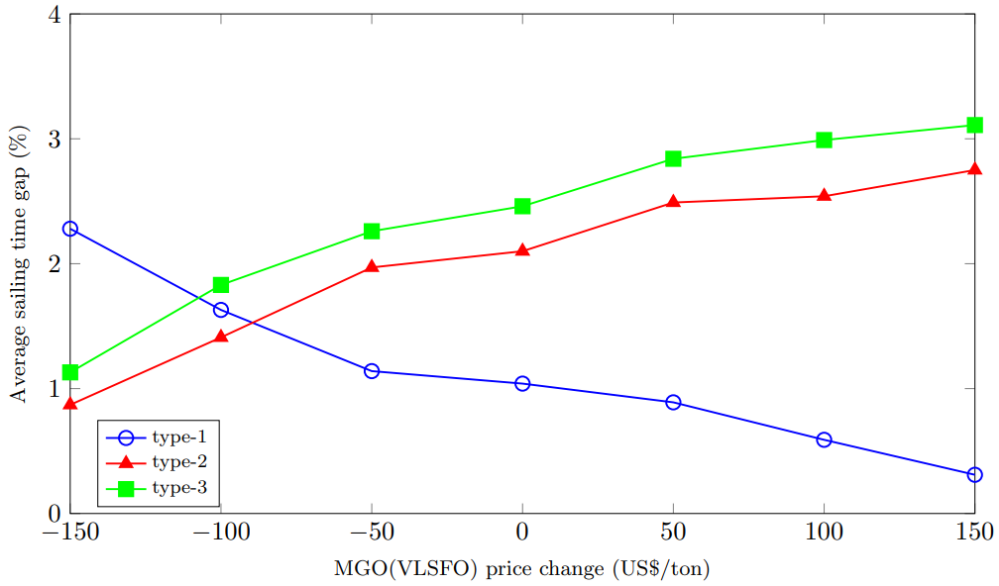

Figure 2 **Impact of MGO(VLSFO) price changes on sailing times**

5.5. Impact of unit carbon emission cost changes on sailing speed

This section examines a five-leg route that includes segments both within and outside ECAs, as well as legs with and without carbon emission costs. We consider four deployment cases: the route served solely by type-1, type-2, or type-3 ships, and a mixed deployment of all three types. For each case, the sailing speeds on every leg—within and outside ECAs—are obtained under different unit carbon emission cost levels.

The results in Table 6 show that Type-1 ships, which operate on MGO and VLSFO, exhibit the largest speed adjustments across legs, because of both the fuel price differences within and

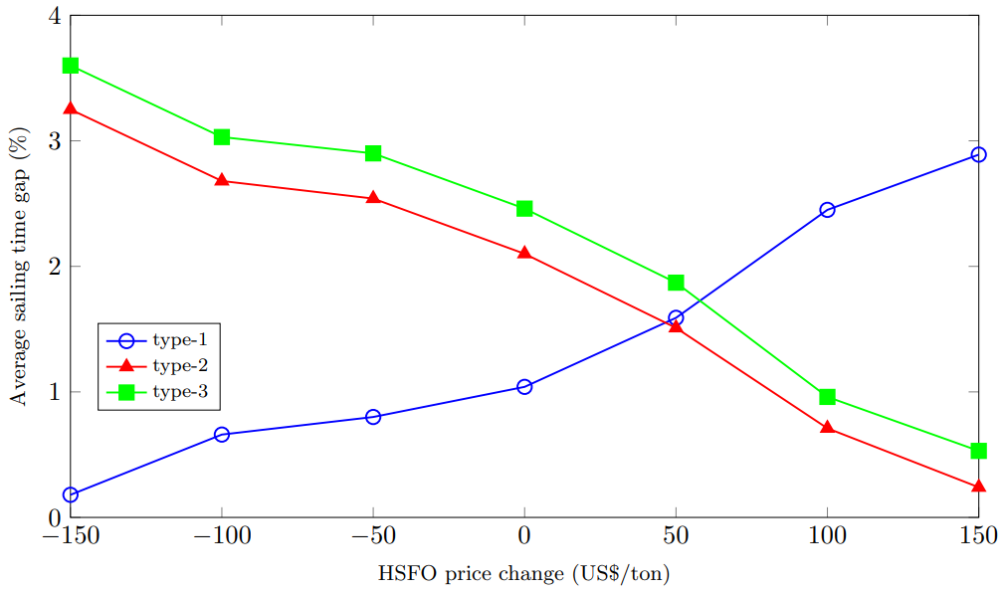

Figure 3 **Impact of HSFO price changes on sailing times**

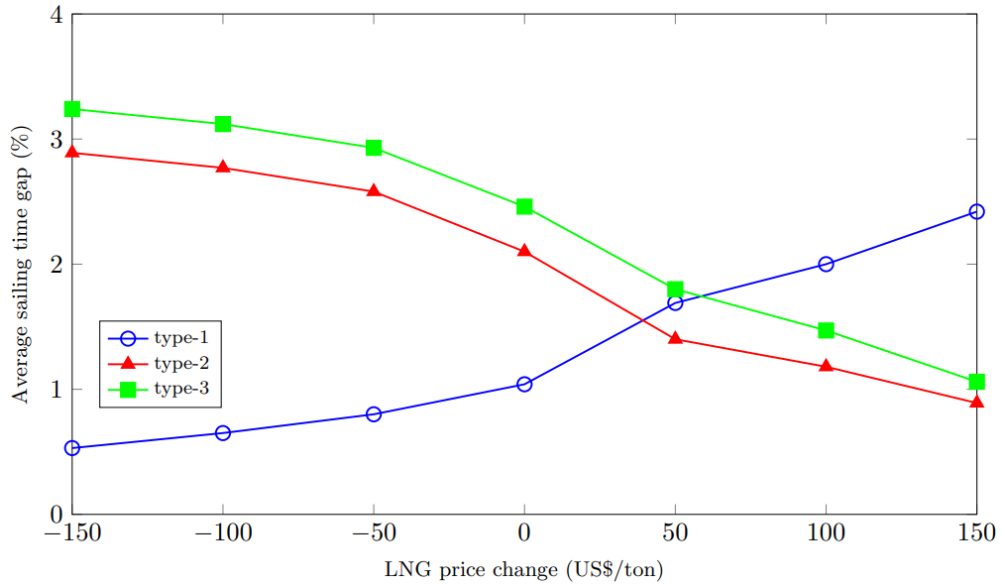

Figure 4 **Impact of LNG price changes on sailing times**

outside ECAs and their relatively high carbon emissions. Type-2 ships running on HSFO also adjust speeds more noticeably than type-3 ships using LNG, due to the higher carbon intensity of HSFO. We further observe that with higher unit carbon emission costs, ships reduce their speeds on charged legs to control cost, which is reflected in the slower speeds on legs 2, 3, and 4. In the mixed-deployment case, the sailing speeds on each leg converge to intermediate values across the three ship types, reflecting the coordinated adjustments needed when multiple ship types operate the same route, which helps maintain economic efficiency.

Table 6 Impact of unit carbon emission cost changes on the speeds of different ship types

Unit carbon emission cost change	Legs	Only type-1 ships		Only type-2 ships	Only type-3 ships	All types of ships			
		Within ECAs	Outside ECAs	Whole leg	Whole leg	Within ECAs (Type-1)	Outside ECAs (Type-1)	Whole leg (Type-2)	Whole leg (Type-3)
	1	0	15.39	15.38	15.23	0	15.33	15.33	15.33
	2	0	14.50	14.27	14.29	0	14.33	14.33	14.33
-20%	3	13.10	13.79	13.42	13.55	12.99	13.67	13.52	13.52
	4	13.68	0	14.27	14.29	14.12	0	14.12	14.12
	5	14.36	15.39	15.38	15.23	14.49	15.53	15.26	15.26
	1	0	15.48	15.49	15.33	0	15.43	15.43	15.43
	2	0	14.49	14.25	14.28	0	14.32	14.32	14.32
-10%	3	13.05	13.71	13.33	13.46	12.93	13.59	13.43	13.43
	4	13.67	0	14.25	14.28	14.10	0	14.10	14.10
	5	14.44	15.48	15.49	15.33	14.58	15.63	15.36	15.36
	1	0	15.56	15.60	15.42	0	15.52	15.52	15.52
	2	0	14.47	14.23	14.26	0	14.30	14.30	14.30
0	3	12.99	13.63	13.24	13.39	12.87	13.50	13.35	13.35
	4	13.67	0	14.23	14.26	14.09	0	14.09	14.09
	5	14.52	15.56	15.60	15.42	14.67	15.73	15.46	15.46
	1	0	15.64	15.70	15.51	0	15.62	15.62	15.62
	2	0	14.45	14.21	14.24	0	14.28	14.28	14.28
10%	3	12.94	13.56	13.16	13.31	12.81	13.42	13.28	13.28
	4	13.67	0	14.21	14.24	14.08	0	14.08	14.08
	5	14.60	15.64	15.70	15.51	14.76	15.82	15.55	15.55
	1	0	15.72	15.80	15.60	0	15.71	15.71	15.71
	2	0	14.43	14.19	14.23	0	14.27	14.27	14.27
20%	3	12.89	13.49	13.09	13.24	12.75	13.34	13.21	13.21
	4	13.67	0	14.19	14.23	14.07	0	14.07	14.07
	5	14.67	15.72	15.80	15.60	14.85	15.91	15.64	15.64

6. Conclusions

This paper explores an integrated fleet deployment and speed optimization problem for liner shipping companies under sulfur and carbon emission regulations. We consider multiple ship

types (three or more) and formulate an MINLP model aimed at minimizing total costs, including fixed ship costs, fuel costs across all routes, and carbon emission costs. Sulfur and carbon emission regulations impose different operational restrictions, leading to varying impacts on both fleet deployment (i.e., the types and number of ships deployed across all routes) and speed optimization. As more ship types are introduced, the number of feasible fleet deployment plans grows sharply, and the resulting heterogeneity in ship characteristics significantly increases the difficulty of speed optimization, thereby further complicating the overall problem. Considering the high complexity of solving the proposed model, we derive valid inequalities to improve computational efficiency and shrink the solution space. To address nonlinearity, we linearize the model using its problem characteristics and a piecewise-linear underestimation approximation. Building on the model properties, we then develop a Benders decomposition algorithm with a tailored cut pool to solve the linearized model, which serves as the foundation for a highly efficient exact algorithm for the original MINLP model.

To evaluate performance, we conduct extensive numerical experiments comparing the proposed exact algorithm with the CPLEX-based benchmark algorithm. The results show that our algorithm consistently yields optimal solutions and significantly outperforms the CPLEX-based algorithm in computational efficiency, achieving nearly a 90-fold speedup. Further comparisons between versions of the proposed exact algorithm, with and without the incorporation of key propositions, indicate that integrating these findings substantially reduces computation time. Beyond algorithmic performance, this study also demonstrates clear practical relevance. The derived structural properties and sensitivity analyses provide managerial insights into how fleet deployment and speed strategies may adapt under different regulatory and market conditions. Through computational experiments based on approximated real-world data, the proposed model and algorithm generate interpretable outputs—such as fleet deployment plans and leg-level sailing speed decisions—for shipping companies operating heterogeneous fleets. Due to the high computational efficiency of the proposed approach, it is applicable even to large-scale liner shipping networks and can support cost-effective operational planning under increasingly stringent sulfur and carbon emission regulations.

References

Chen, J., Jia, S., Wang, S., Liu, Z., 2018a. Subloop-based reversal of port rotation directions for container liner shipping network alteration. Transportation Research Part B: Methodological 118, 336–361.

Chen, L., Yip, T.L., Mou, J., 2018b. Provision of emission control area and the impact on shipping route choice and ship emissions. Transportation Research Part D: Transport and Environment 58, 280–291.

Cheng, L., Xu, L., Bai, X., 2025. Cargo selection, route planning, and speed optimization in tramp shipping under carbon intensity indicator (CII) regulations. Transportation Research Part E: Logistics and Transportation Review 194, 103948.

Christiansen, M., Hellsten, E., Pisinger, D., Sacramento, D., Vilhelmsen, C., 2020. Liner shipping network design. European Journal of Operational Research 286, 1–20.

Du, Y., Meng, Q., Wang, S., Kuang, H., 2019. Two-phase optimal solutions for ship speed and trim optimization over a voyage using voyage report data. Transportation Research Part B: Methodological 122, 88–114.

Fagerholt, K., Psaraftis, H.N., 2015. On two speed optimization problems for ships that sail in and out of emission control areas. Transportation Research Part D: Transport and Environment 39, 56–64.

Ge, F., Beullens, P., Hudson, D., 2021. Optimal economic ship speeds, the chain effect, and future profit potential. Transportation Research Part B: Methodological 147, 168–196.

Gu, Y., Wallace, S., 2017. Scrubber: A potentially overestimated compliance method for the emission control areas: The importance of involving a ship's sailing pattern in the evaluation. Transportation Research Part D: Transport and Environment 55, 51–66.

Lee, C.Y., Song, D.P., 2017. Ocean container transport in global supply chains: Overview and research opportunities. Transportation Research Part B: Methodological 95, 442–474.

Lee, S.J., Sun, Q., Meng, Q., 2023. Vessel weather routing subject to sulfur emission regulation. Transportation Research Part E: Logistics and Transportation Review 177, 103235.

Luo, X., Yan, R., Wang, S., 2024. Ship sailing speed optimization considering dynamic meteorological conditions. Transportation Research Part C: Emerging Technologies 167, 104827.

Ma, W., Zhang, J., Han, Y., Mao, T., Ma, D., Zhou, B., Chen, M., 2023. A decision-making optimization model for ship energy system integrating emission reduction regulations and scheduling strategies. Journal of Industrial Information Integration 35, 100506.

Meng, Q., Wang, S., Andersson, H., Thun, K., 2014. Containership routing and scheduling in liner shipping: Overview and future research directions. Transportation Science 48, 265–280.

MI-News-Network, 2017. Maersk triple-E vessels: Why size matters? URL: `https://www.marineinsight.com/shipping-news/size-matters/`. Accessed on 20 July 2024.

Ng, M., Lin, D.Y., 2018. Fleet deployment in liner shipping with incomplete demand information. Transportation Research Part E: Logistics and Transportation Review 116, 184–189.

Park, H., Blanco, C.C., Bendoly, E., 2022. Vessel sharing and its impact on maritime operations and carbon emissions. Production and Operations Management 31, 2925–2942.

Qi, X., Song, D.P., 2012. Minimizing fuel emissions by optimizing vessel schedules in liner shipping with uncertain port times. Transportation Research Part E: Logistics and Transportation Review 48, 863–880.

Rennert, K., Errickson, F., Prest, B.C., Rennels, L., Newell, R.G., Pizer, W., Kingdon, C., Wingenroth, J., Cooke, R., Parthum, B., et al., 2022. Comprehensive evidence implies a higher social cost of CO_2. Nature 610, 687–692.

Seatrade-ShipTech-Middle-East, 2019. Triple-E class container ships. URL: `https://www.shiptechnology.com/projects/triple-e-class/`. Accessed on 20 July 2024.

Shao, S., Xu, M., Tan, Z., Zhen, L., 2024. Ship deployment problem with green technology adoption for an inland river carrier under non-identical streamflow and speed limits. Transport Policy 157, 46–56.

Ship, Bunker, 2024. World bunker prices. URL: `https://shipandbunker.com/prices`. Accessed on 28 December 2024.

UNCTAD, 2023. Review of Maritime Transport 2023. Paper presented at the United Nations Conference on Trade and Development, New York and Geneva. URL: `https://unctad.org/system/files/official-document/rmt2023_en.pdf`. Accessed on 27 February 2025.

Wang, S., Meng, Q., 2012. Sailing speed optimization for container ships in a liner shipping network. Transportation Research Part E: Logistics and Transportation Review 48, 701–714.

Wang, S., Wang, X., 2016. A polynomial-time algorithm for sailing speed optimization with containership resource sharing. Transportation Research Part B: Methodological 93, 394–405.

Wang, S., Zhao, Q., 2022. Probabilistic tabu search algorithm for container liner shipping problem with speed optimisation. International Journal of Production Research 60, 3651–3668.

Wang, S., Zhuge, D., Zhen, L., Lee, C.Y., 2021. Liner shipping service planning under sulfur emission regulations. Transportation Science 55, 491–509.

Wang, T., Cheng, P., Wang, Y., 2025a. How the establishment of carbon emission trading system affects ship emission reduction strategies designed for sulfur emission control area. Transport Policy 160, 138–153.

Wang, T., Li, S., Zhen, L., Zhao, T., 2025b. The reliable ship fleet planning problem for liner shipping services. Transportation Research Part E: Logistics and Transportation Review 193, 103856.

Wang, Y., Wang, S., 2021. Deploying, scheduling, and sequencing heterogeneous vessels in a liner container shipping route. Transportation Research Part E: Logistics and Transportation Review 151, 102365.

Wang, Y., Zhang, H., Wang, T., Liu, J., 2025c. Heterogeneous vessel fleet co-management for liner alliances under profit-sharing agreement and weekly-dependent demand. Transportation Research Part E: Logistics and Transportation Review 194, 103880.

Wetzel, D., Tierney, K., 2020. Integrating fleet deployment into liner shipping vessel repositioning. Transportation Research Part E: Logistics and Transportation Review 143, 102101.

Wu, Y., Wang, S., Zhen, L., Laporte, G., Tan, Z., Wang, K., 2023. How to operate ship fleets under uncertainty. Production and Operations Management 32, 3043–3061.

Xiang, X., Xu, X., Liu, C., Jia, S., 2024. Liner fleet deployment and empty container repositioning under demand uncertainty: A robust optimization approach. Transportation Research Part B: Methodological 190, 103088.

Zeng, X., Tan, Z., Zhang, M., Wang, T., 2024. Scrubber installation of inland container ships: Discrepancy between government and carriers. Transportation Research Part E: Logistics and Transportation Review 186, 103543.

Zhang, M., Zeng, X., Tan, Z., 2024a. Joint decision of green technology adoption and sailing pattern for a coastal ship under ECAs. Transport Policy 146, 102–113.

Zhang, Q., Guan, H., Chen, S., Wan, Z., 2024b. Towards decarbonization: How eexi and cii regulations affect container liner fleet deployment. Transportation Research Part D: Transport and Environment 133, 104277.

Zhao, S., Yang, H., Zheng, J., Li, D., 2024. A two-step approach for deploying heterogeneous vessels and designing reliable schedule in liner shipping services. Transportation Research Part E: Logistics and Transportation Review 182, 103416.

Zhen, L., Hu, Y., Wang, S., Laporte, G., Wu, Y., 2019. Fleet deployment and demand fulfillment for container shipping liners. Transportation Research Part B: Methodological 120, 15–32.

Zhen, L., Wu, Y., Wang, S., Laporte, G., 2020. Green technology adoption for fleet deployment in a shipping network. Transportation Research Part B: Methodological 139, 388–410.

Zhen, L., Zhuge, D., Zhang, S., Wang, S., Psaraftis, H.N., 2024. Optimizing sulfur emission control areas for shipping. Transportation Science 58, 614–638.

Zhou, R., Luo, M., Jiang, C., Yang, D., Wang, K., 2025. How does emission allowance allocation affect shipowners' selection of emission reduction technologies? Transportation Research Part D: Transport and Environment 139, 104573.

Zhuge, D., Wang, S., Wang, D.Z., 2021. A joint liner ship path, speed and deployment problem under emission reduction measures. Transportation Research Part B: Methodological 144, 155–173.

Zhuge, D., Wang, S., Zhen, L., 2024. Shipping emission control area optimization considering carbon emission reduction. Operations research 72, 1333–1351.

Zhuge, D., Wang, S., Zhen, L., Laporte, G., 2020. Schedule design for liner services under vessel speed reduction incentive programs. Naval Research Logistics 67, 45–62.

Zis, T.P., Cullinane, K., Ricci, S., 2022. Economic and environmental impacts of scrubbers investments in shipping: a multi-sectoral analysis. Maritime Policy & Management 49, 1097–1115.